Journal of Electrochemistry

Volume 28
Issue 2 *Special Issue: Frontier of Electrochemistry (I)*

2022-02-28

A Beginners' Guide to Modelling of Electric Double Layer under Equilibrium, Nonequilibrium and AC Conditions

Lu-Lu Zhang

Chen-Kun Li

Jun Huang
3. Institute of Theoretical Chemistry,Ulm University, 89069 Ulm Germany;, jhuangelectrochem@qq.com

电 化 学
J. Electrochem. 2022, 28(2), 2108471 (1 of 30)

【Protocol】 **DOI**: 10.13208/j.electrochem.210847 **Http**://electrochem.xmu.edu.cn

A Beginners' Guide to Modelling of Electric Double Layer under Equilibrium, Nonequilibrium and AC Conditions

Lu-Lu Zhang[1#], Chen-Kun Li[2#], Jun Huang[3*]

(*1. School of Chemistry and Materials Science, University of Science and Technology of China, Hefei 230026, Anhui, People's Republic of China; 2. College of Chemistry and Chemical Engineering, Central South University, Changsha 410083, Hunan, People's Republic of China; 3. Institute of Theoretical Chemistry,Ulm University, 89069 Ulm Germany*)

Abstract: In electrochemistry, perhaps also in other time-honored scientific disciplines, knowledge labelled classical usually attracts less attention from beginners, especially those pressured or tempted to quickly jam into research fronts that are labelled, not always aptly, modern. In fact, it is a normal reaction to the burden of history and the stress of today. Against this context, accessible tutorials on classical knowledge are useful, should some realize that taking a step back could be the best way forward. This is the driving force of this article themed at physicochemical modelling of the electric (electrochemical) double layer (EDL). We begin the exposition with a rudimentary introduction to key concepts of the EDL, followed by a brief introduction to its history. We then elucidate how to model the EDL under equilibrium, using firstly the orthodox Gouy-Chapman-Stern model, then the symmetric Bikerman model, and finally the asymmetric Bikerman model. Afterwards, we exemplify how to derive a set of equations governing the EDL dynamics under nonequilibrium conditions using a unifying grand-potential approach. In the end, we expound on the definition and mathematical foundation of electrochemical impedance spectroscopy (EIS), and present a detailed derivation of an EIS model for a simple EDL. We try to avoid the omission of supposedly 'trivial' information in the derivation of models, hoping that it can ease the access to the wonderful garden of physical electrochemistry.

Key words: electric double layer; equilibrium; nonequilibrium; electrochemical impedance spectroscopy

1 Introduction

1.1 What is An Electric Double Layer?

An electrochemical cell has two electrodes separated by an electrolyte solution, as schematically shown in Figure 1. The electric potential difference between the two electrodes, denoted V_{cell}, can be modulated with a potentiostat at one's disposal. By varying V_{cell}, one gets a handle on controlling the difference in the electrochemical potential of electrons between the two electrodes. Electrons flow from the electrode with the higher electrochemical potential (lower electric potential), via the potentiostat, to the other side. Let us consider for the moment ideally polarizable electrodes. The resultant electron flow cannot cross the electrode-electrolyte interface (EEI) regardless of V_{cell}. Therefore, excess or deficient electrons, corresponding to a net negative or positive surface charge, are distributed over a skin layer of several angstroms (Å) thick on the electrode surface, which is a consequence of quantum-mechanical behaviors of electrons. Counterions are attracted to and coions are repelled from

Cite as: Zhang L L, Li C K, Huang J. A beginners' guide to modelling of electric double layer under equilibrium, nonequilibrium and ac conditions. *J. Electrochem.*, 2022, 28(2): 2108471.

Received: 2021-10-26, Revised: 2021-12-07. #Equal contribution. *Corresponding author, Tel: (+49)15906819204, E-mail: jhuangelectrochem@qq.com

the electrode surface via electrostatic interactions, as illustrated in Figure 1. In addition, the solvent molecules adjust their orientation according to the strong electric field generated by the net surface charge. These coupled phenomena occur in a non-electroneutral region of a few nanometer (nm) thick, which is termed as the electric double layer (EDL).

In most cases, the electron flow can cross the EEI, resulting in oxidation or reduction of solution species near the electrode. The electron transfer rate depends on the distributions of the electric potential, the concentrations of reactant and product, and the dielectric polarization of the solvation environment. Therefore, the structure and properties of the EDL are important factors influencing interfacial electron transfer reactions.

1.2 Key Properties of the EDL

The distributions of the electric potential, the ion concentrations, and the solvent orientation in the EDL are dictated by the excess surface charge density, denoted σ_M. In an electrochemical cell, the two electrodes have σ_M of the same magnitude but opposite signs, because the full cell must be electroneutral. σ_M can be varied as a function of V_{cell}, or as long as a single electrode is considered, σ_M is a function of the electric potential, ϕ_M, of the considered electrode. The relation between σ_M and ϕ_M is called *surface charging relation*. Determining the σ_M - ϕ_M relation is an essential task in modelling the EDL and electrochemical reactions therein.

A schematic illustration of the surface charging relation of the EDL is given in Figure 2. The electric potential in the bulk solution, ϕ_S, is taken as the reference. The electric potential in the electrode bulk, ϕ_M, can be adjusted at will. There is a potential drop, χ, on the electrode surface, which is caused by electron spillover from the solid electrode into the electrolyte solution[1]. χ is related to the electron density of the solid electrode, therefore, its value depends on how many electrons are included in the calculation. More specifically, χ is much higher if more electrons of the metal are considered explicitly. For a given metal, χ varies slightly with ϕ_M, and we assume that χ is a constant in the subsequent analysis.

Consider first the case of $\phi_M - \phi_S < \chi$, as shown in Figure 2(A). The electric potential in the electrolyte solution near the electrode surface is lower than ϕ_S. Therefore, cations are accumulated in the EDL because they have a lower energy there. Contrarily, anions are depleted. Hence, a positive net charge is stored in the EDL, which is accompanied by excess electrons on the metal surface and $\sigma_M < 0$. If ϕ_M is increased, the electric potential in the EDL becomes more positive because we assume a constant χ for the electrode. This means that less cations are accumulated and less anions are repelled in the EDL. Therefore, σ_M becomes less negative and shifts

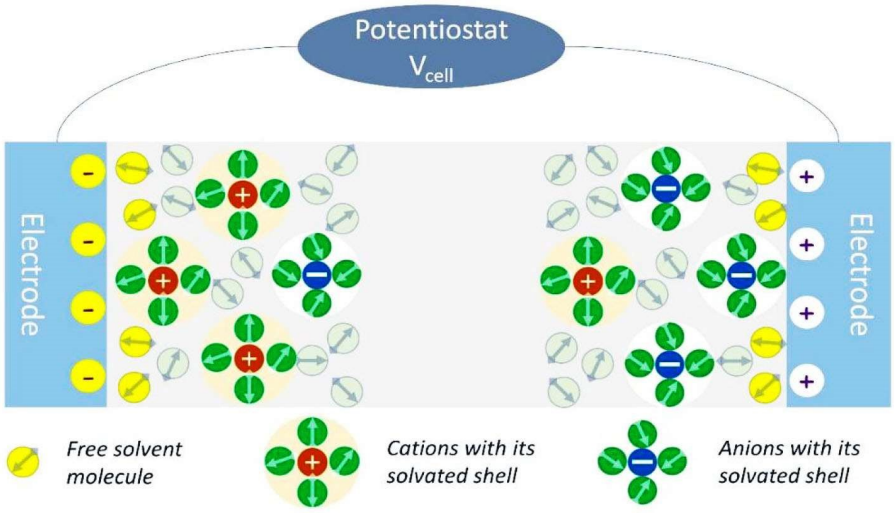

Figure 1 An electrochemical cell with two charged electrode/electrolyte interfaces. (color on line)

towards more positive values.

For the case of $\phi_M - \phi_S = \chi$, as illustrated in Figure 2(B), the electric potential in whole electrolyte solution is zero as we have set the potential reference in the bulk solution. There is no excess charge in the EDL or on the electrode surface, i.e., $\sigma_M = 0$. This particular value of ϕ_M is the *potential of zero charge* (pzc)[2]. For the case of $\phi_M - \phi_S > \chi$, shown in Figure 2(C), anions are accumulated and cations are depleted in the EDL, i.e., $\sigma_M > 0$. Overall, the $\sigma_M - \phi_M$ relation shows a monotonically increasing trend for ordinary EDLs. From this relation, we obtain the *differential double-layer capacitance* C_{dl},

$$C_{dl} = \frac{\partial \sigma_M}{\partial \phi_M} \tag{1}$$

For EDLs with chemisorption, the surface charging relation can be nonmonotonic. In Figure 2, we give such an example, where chemisorption occurs in the high potential range. The chemisorbates are usually partially charged due to the partial charge transfer[3]. The charged chemisorbates, together with the compensating charge located on metal surface atoms, give rise to a surface dipole moment, which is termed the chemisorption-induced surface dipole moment, μ_{chem}. μ_{chem} introduces an additional contribution to the potential drop on the electrode surface, $\Delta\chi$. Even at a high potential $\phi_M - \phi_S > \chi$, the electrode surface with chemisorbates could be negatively charged due to the additional negative potential drop $\Delta\chi$. Consequently, the surface charging relation could be nonmonotonic with a *second pzc* in the high potential region for electrocatalytic interfaces[4, 5]. According to its definition, C_{dl} is negative in the nonmonotonic region of the $\sigma_M - \phi_M$ relation. Note that in the presence of chemisorbates, the definition of σ_M should be varied accordingly, which contains not only the excess charge on the electrode surface, but also the net charged carried on the charged adsorbates. In this regard, it is better to be denoted σ_{free}.

1.3 Purpose and Structure of This Paper

We wish to provide a tutorial for physical modelling of the EDL under both equilibrium and nonequilibrium conditions. Both time-domain and frequency-domain responses are modelled under nonequilibrium conditions. The latter is in fact the electrochemical impedance response. As a tutorial, this paper includes a systematic exposition of relevant models with mathematical details provided. We also provide simulation scripts of these models

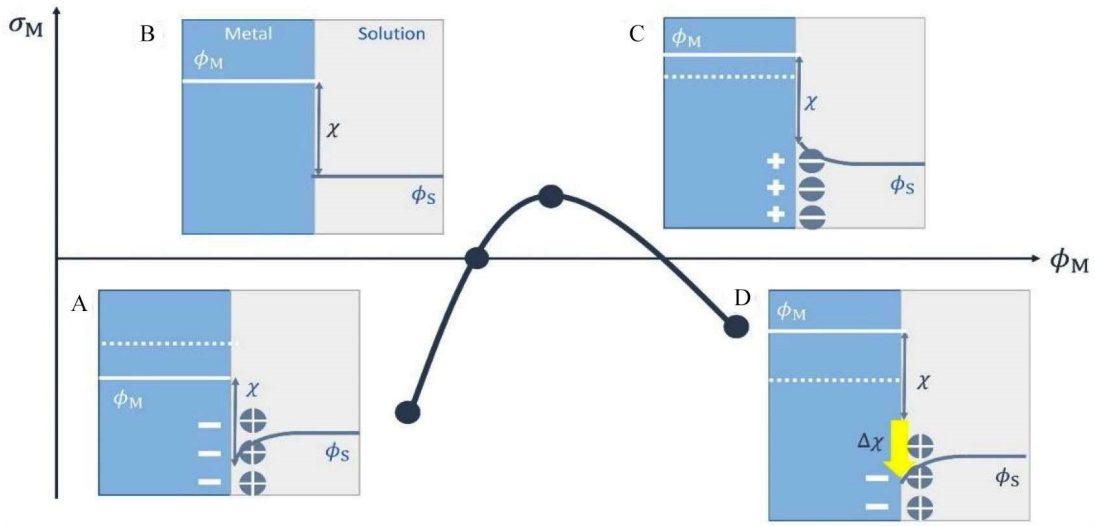

Figure 2 Surface charging relation: (A) $\phi_M - \phi_S < \chi$, (B) $\phi_M - \phi_S = \chi$, (C) $\phi_M - \phi_S > \chi$, and (D) with an additional potential drop $\Delta\chi$ at the surface due to chemisorption-induced surface dipole. In the presence of chemisorption, σ_M contains not only the excess charge on the electrode surface, but also the net charged carried on the charged adsorbates. (color on line)

in the supporting information.

The remaining parts of this paper are organized as follows. We first provide a brief history of the EDL theory. Then, we introduce EDL models under equilibrium conditions, including the Gouy-Chapman-Stern model, then the Bikerman model that takes ion size effects into account, and finally a modified Bikerman model that considers asymmetric ion size effects. Next, we derive nonequilibrium EDL models from a grand potential of the EDL. Afterwards, we present the basics of EIS, and demonstrate how to derive an EIS model from the nonequilibrium EDL models.

2 A Brief History of the EDL Theory

A quantitative determination of the $\sigma_M = f(\phi_M)$ relation requires a physicochemical model for the EDL. Figure 3 summarizes milestones in the evolution of EDL modelling and simulations. Helmholtz (1879) viewed the EDL as a planar plate capacitor with a constant double-layer capacitance (C_{dl}) and a linear potential distribution in the space between two plates[6]. Different from Helmholtz who assumed a rigid lining up of counterions, Gouy and Chapman considered the diffuse nature of counterions in the electrolyte solution in 1910[7, 8], ten years before Debye and Hückel. In the Gouy-Chapman model, the electrolyte solution is viewed as a cloud of point ions embedded in a dielectric continuum. The distributions of the electric potential and ion concentrations are governed by the Poisson-Boltzmann equation. The Gouy-Chapman model is limited to very dilute solutions at slightly charged interfaces due to its foundation on the point charge assumption. At highly charged interfaces or when ϕ_M is shifted far away from the pzc, the Gouy-Chapman model results in an unphysically high concentration of counterions near the electrode surface. Under such scenarios, the gap between the electrode surface and the midplane of the diffuse layer, denoted d_0, becomes very small, leading to the phenomenon of capacity catastrophe, namely, C_{dl} grows toward infinity.

Stern removed this limitation by constraining the closest approach of counterions to the Helmholtz plane (HP)[9]. This way, regardless of the magnitude of surface charge density on the electrode, d_0 has a lower limit, thus turning the catastrophic growth of C_{dl} when ϕ_M is shifted away from the pzc into a leveling off region. Bikerman furthered the consideration of ion size effects using a lattice-gas model[10]. There is a delicate difference regarding the consideration of ion size in Stern's and Bikerman's treatments. Although d_0 is constrained in the Stern model, the Poisson-Boltzmann equation is inherited. This means that the ion concentration at the HP and in the diffuse layer can be infinite in the Stern model. In contrast, in the Bikerman model, the ion concentration at the HP and in the diffuse layer has a finite upper limit determined by the lattice size. Consequently, in the Bikerman model, d_0 first narrows down due to counterion crowding and then expands due to counterion overcrowding, when ϕ_M is shifted away from the pzc. Consequently, a camel-shaped double-layer capacitance profile is usually obtained. In highly concentrated solutions, a bell-shaped double-layer capacitance profile is obtained, as d_0 always increases when ϕ_M is shifted away from the pzc.

Grahame extended Stern's idea in the presence of specific adsorption of ions[11]. He divided the HP into an inner HP (IHP) where specifically adsorbed ions reside and an outer HP (OHP) where solvated counterions reside. It was implicitly assumed that the specifically adsorbed ions retain the charge they have in the bulk solution, which was later corrected by the concept of partial charge transfer by Lorenz and Salie in 1961[12]. Moreover, as a first approximation, the potential distribution in the inner layer is considered to be linear. The potential difference across the inner layer is composed of two contributions. One is caused by the net surface charge on the electrode surface, denoted σ_M. The other is caused by the charge carried by the specifically adsorbed ions. Grahame calculated the differential capacitance of the inner layer (C_{IHP}) as a function of σ_M[13]. C_{IHP} is asymmetric and humped with a maximum at positive σ_M. Grahame's results aroused wide interests among theorists, suggesting

two new lines of EDL modelling, namely, description of water dipoles at the IHP and description of metal electrons, which are detailed below.

Grahame spent his sabbatical year in 1958/59 in Britain and had a fruitful collaboration with Roger Parsons. This British visit disseminated his experimental findings among physicists at Cambridge. Watts-Tobin and Mott tried to interpret the rise of C_{IHP} for anodic polarizations and the hump of C_{IHP} at a ϕ_M slightly positive to the pzc[14]. The former phenomenon had been controversial, plausible causes including adsorption of mercury ions, specifically adsorbed hydroxyl ions, potential varying distance between the OHP and the metal surface, among others[15]. The latter phenomenon is ascribed to the orientational polarization of interfacial water molecules, which was initially suggested by Grahame and latter modelled by Watts-Tobin[16]. Watts-Tobin assumed that interfacial water molecules may occupy two states (H-down or O-down). The basic idea is that interfacial water molecules are more polarized at more charged surface, resulting in a decreased permittivity and lower C_{IHP}. Consequently, the hump of C_{IHP} is located at the pzc where the permittivity of water molecules is maximum. The deviation of the hump from the pzc observed in experiments is caused by the 'natural field' on the metal surface, namely, metal electronic effects, which became a hot topic in 1980s[17]. The Watts-Tobin model had been refined in several rounds by considering more states of water and the hydrogen-bond network, see a review by Guidelli and Schmickler[18].

Together with Grahame's data of C_{IHP} that gave the first hint of the importance of metal electronic effects, Trasatti's correlation between C_{IHP} of simple sp metals taken at the pzc and the metal electron density drove theorists to explicitly consider the metal electronic effects[19]. In 1980s, Schmickler, Badiali, Kornyshev and their associates introduced the jellium model that had been widely used in the theory of metal surfaces to the EDL theory[20-22]. In the jellium model, the metal is treated as an inhomogeneous electron gas situated against a positive background charge corresponding to metal cationic cores. The electron gas was described using local density approximations, such as the Thomas-Fermi-von Weizsäcker theory[23]. The positive background charge was later replaced with pseudopotentials to consider metal specific behaviors. The jellium model is able to rationalize the metal and surface-charge dependence of C_{IHP}[17].

The next milestone in the EDL modelling is the work of Price and Halley in 1995[24]. They adopted the Car-Parrinello method of combining molecular dynamics and density functional theory (DFT) to simulate the EDL formed at a copper slab and water molecules. This work opened up a new direction in atomistic modelling of the EDL. Since then, the field has been shifted to extensive computer simulations with the Kohn-Sham DFT at the core. Most DFT-based first-principles simulations have been conducted for electroneutral interfaces. In 2006, Otani and Sugino developed a method to simulate charged interfaces[25]. They employed the Poisson-Boltzmann equation for the electrolyte solution to screen excess charge on the metal slabs. This so-called implicit solvation method was subsequently advanced by several groups of authors, including Arias et al.[26-28], Jinnouchi and Anderson[29], Hennig et al.[30, 31], Nishihara and Otani[32], Marzari et al.[33, 34], and Melander et al.[35] Recent *ab initio* molecular dynamics (AIMD) simulations were able to handle the charged solid electrodes by introducing ions into the solvent layers [36-39]. This provides a means to properly treat the electrode potential which is calculated from the work function of the system referenced to a (computational) standard hydrogen electrode (SHE).

Recently, Huang and coworkers developed a hybrid density-potential functional theory (DPFT) for the EDL, combining quantum mechanical treatment of many electrons and classical statistical treatment of charged particles in the solution phase[1, 40, 41]. The DPFT avoids the calculation of Kohn-Sham orbitals which is computationally expensive. Instead, the DPFT is based on so-called orbital-free DFT[42-44]. This feature distinguishes the DPFT model from other DFT-based first principles models, such as the joint DFT model for the EDL developed by Arias et al[27, 28]. In Refs.[1, 41], the orbital-free DFT for metal electrodes consists of the Thomas-Fermi-von Weizsäcker

theory for the electronic kinetic energy, a rudimentary kinetic energy density functional (KEDF), and the Dirac-Wigner theory for the exchange-correlation functional, a rudimentary local density approximation. As for the electrolyte solution, Huang developed a statistical field theory considering asymmetric steric effects, solvent polarization, and ion-specific interactions with the metal[41]. Combined, a hybrid density-potential functional for the grand potential functional of the EDL is obtained. Variational analysis of this functional yields a grand-canonical EDL model described by two Euler-Lagrange equations in terms of the electron density and the electric potential.

3 Equilibrium Models

3.1 Gouy-Chapman-Stern Model

The Gouy-Chapman-Stern (GCS) model is a classical toy model of the EDL. The electric potential distributes linearly from the electrode to the HP, and is described by Poisson-Boltzmann (PB) equation in the diffuse layer and the diffusion layer as shown in the third subfigure in Figure 3. The distance from the electrode to the HP is usually taken as the radius of a hydrated ion.

The PB equation describes the distributions of the electric potential and the ion concentrations in the electrolyte solution. Poisson equation reads,

$$\nabla(\epsilon_s \nabla \phi) = -\sum_i z_i F c_i \tag{2}$$

where ϵ_s is the dielectric permittivity of the bulk solution, ϕ the electric potential referenced to the electric potential in the bulk solution, ϕ_S, z_i the charge number of ion i, F the Faraday's constant, c_i the concentration of ion i. Boltzmann equation further connects c_i and ϕ,

$$c_i = c_i^{b} \exp\left(-\frac{z_i F}{RT}\phi\right) \tag{3}$$

where c_i^{b} is the concentration of ion i in the bulk solution, R the gas constant, T the absolute temperature. For a monovalent electrolyte solution in a one-dimensional space, the PB equation is rewritten as,

$$\frac{\partial^2 \phi}{\partial x^2} = -\frac{F c^{b}}{\epsilon_s}\left(\exp\left(-\frac{F\phi}{RT}\right) - \exp\left(\frac{F\phi}{RT}\right)\right) \tag{4}$$

where c^{b} the concentration of total anions (cations) in the bulk solution. The dimensionless form of the PB equation is written as,

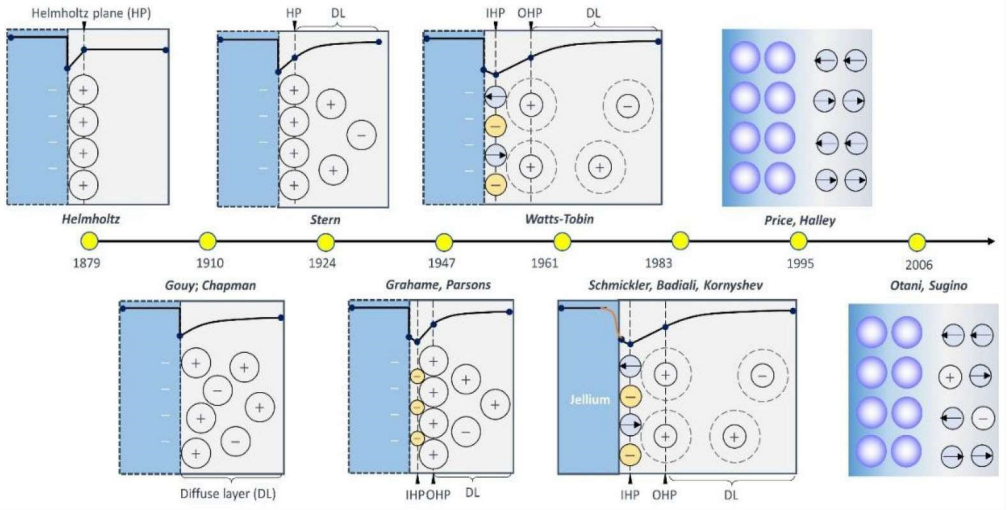

Figure 3 Key milestones of EDL modelling (color on line)

$$\frac{\partial^2 U}{\partial X^2} = \sinh(U) \tag{5}$$

with the dimensionless quantities, $U = F\phi/RT$, $X = x/\lambda_D$, and the Debye length $\lambda_D = \sqrt{RT\epsilon_s/2F^2c^b}$. Note that the dielectric permittivity depends on the local density of solvent molecules and the local electric field. In an aqueous electrolyte solution, the dielectric permittivity is a multiple of ϵ_0 inside the HP, and increases to $78.5\epsilon_0$ in the bulk solution. Therefore, different values of the dielectric permittivity are used on the two sides of the HP.

The boundary conditions to close Eq.(5), a second-order differential equation, are,

$$U(X = 0) = U_{HP} \tag{6}$$

$$U(X = \infty) = 0 \tag{7}$$

where $X = 0$ represents the left boundary at the HP, and $X = \infty$ is the right boundary in the bulk solution. ϕ_{HP}[4] (dimensional quantity of U_{HP}) can be calculated from the electrode side by,

$$\phi_{HP} = \phi_M - \phi_{pzc} + \left(\frac{\partial \phi}{\partial x}\right)_{x=0^+} \frac{\epsilon_s}{\epsilon_{HP}} \delta_{HP} \tag{8}$$

where ϕ_{HP} is the electric potential at the HP, ϕ_M the electrode potential, ϕ_{pzc} the potential of zero charge (note that this is not the absolute potential drop at the electrode surface, but the one relative to that of a reference electrode which is a constant), ϵ_{HP} and δ_{HP} are the dielectric permittivity and the thickness of the space between the

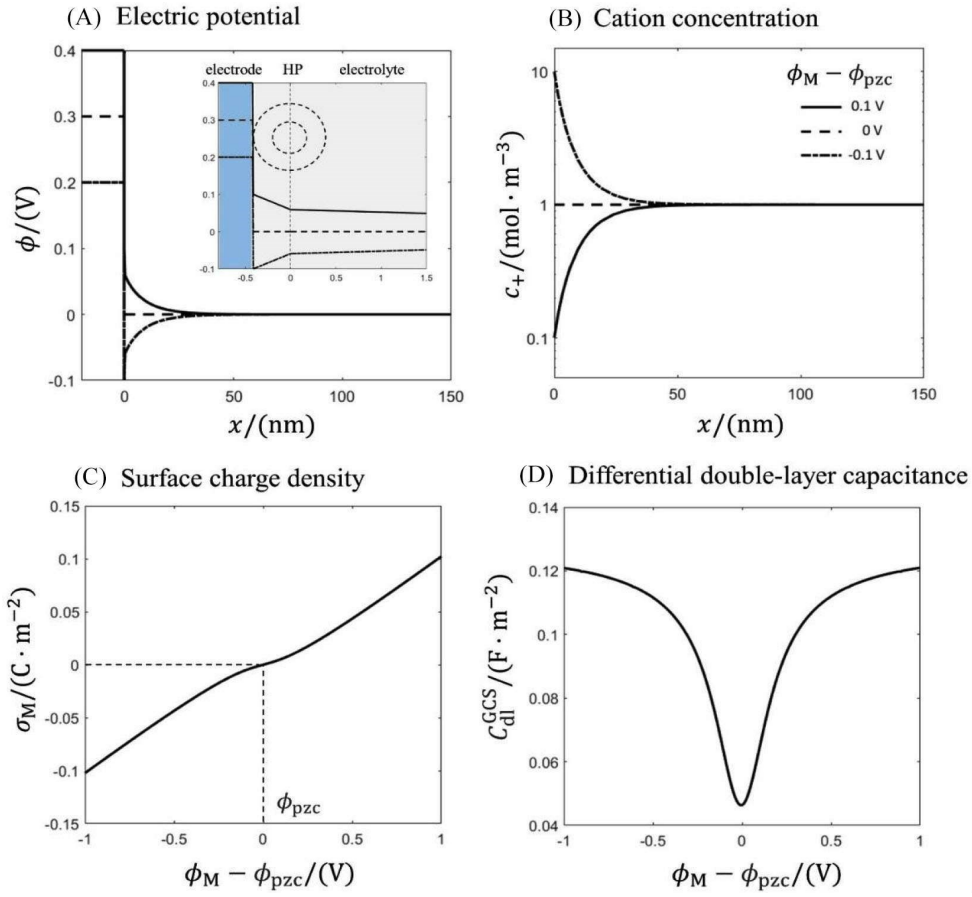

Figure 4 Typical results of the GCS model, including the spatial distributions of (A) the electric potential and (B) the cation concentration, and the relationships between (C) the surface charge density and (D) the differential double-layer capacitance with the electrode potential. The inset in (A) illustrates the electric potential distribution within 2 nm near the electrode. The parameters for calculation are listed in Table 1. Matlab script of this model is provided in the supporting information. (color on line)

electrode and the HP, respectively. The coefficient ϵ_s/ϵ_{HP} is resultant from the following equality in terms of surface charge density on the electrode surface,

$$\sigma_M = -\epsilon_s\left(\frac{\partial\phi}{\partial x}\right)_{x=0^+} = -\epsilon_{HP}\left(\frac{\partial\phi}{\partial x}\right)_{x=0^-} \tag{9}$$

Solving Eq. (5) in the following steps,

$$2\frac{\partial^2 U}{\partial X^2}\frac{\partial U}{\partial X} = 2\sinh(U)\frac{\partial U}{\partial X} \tag{10}$$

$$\mathrm{d}\left(\frac{\partial U}{\partial X}\right)^2 = \mathrm{d}(2\cosh U) \tag{11}$$

$$\left(\frac{\partial U}{\partial X}\right)_{X=0^+}^2 = \left(2\sinh\left(\frac{U_{HP}}{2}\right)\right)^2 \tag{12}$$

we obtain the relationship between the surface charge density and the electric potential at the HP,

$$\sigma_M = -\int (c_+ - c_-)F\mathrm{d}x = -\epsilon_s\left(\frac{\partial\phi}{\partial x}\right)_{x=0^+} = \frac{2\epsilon_s RT}{F\lambda_D}\sinh\left(\frac{F\phi_{HP}}{2RT}\right) \tag{13}$$

Bvp4c is a convenient built-in tool in Matlab for solving boundary value problems described as ordinary differential equations. In accord with the syntax of this tool, Eq. (5) is rewritten as,

$$\frac{\partial U}{\partial X} = Y \tag{14}$$

$$\frac{\partial Y}{\partial X} = \sinh(U) \tag{15}$$

where $Y = \frac{F\lambda_D}{RT}\frac{\partial\phi}{\partial x}$ is the dimensionless electric field strength.

Figure 4 shows the typical results of the GCS model (the Matlab script is provided in the supporting information of this article), including the spatial distributions of the electric potential, ϕ, and the cation concentration, c_+, at a series of ϕ_M in (A) and (B), and the relationships between the surface charge density, σ_M, and the differential double-layer capacitance, C_{dl}, with ϕ_M, in (C) and (D). The spatial range for calculation is 150 nm from the HP. When $\phi_M - \phi_{pzc} > 0$, we find $\phi_{HP} > 0$, $\sigma_M > 0$, and cations are repelled. When $\phi_M - \phi_{pzc} = 0$, we obtain $\phi_{HP} = 0$, $\sigma_M = 0$. When $\phi_M - \phi_{pzc} < 0$, we get $\phi_{HP} < 0$, $\sigma_M < 0$, and cations are attracted. As defined in Eq.(1), C_{dl} has the

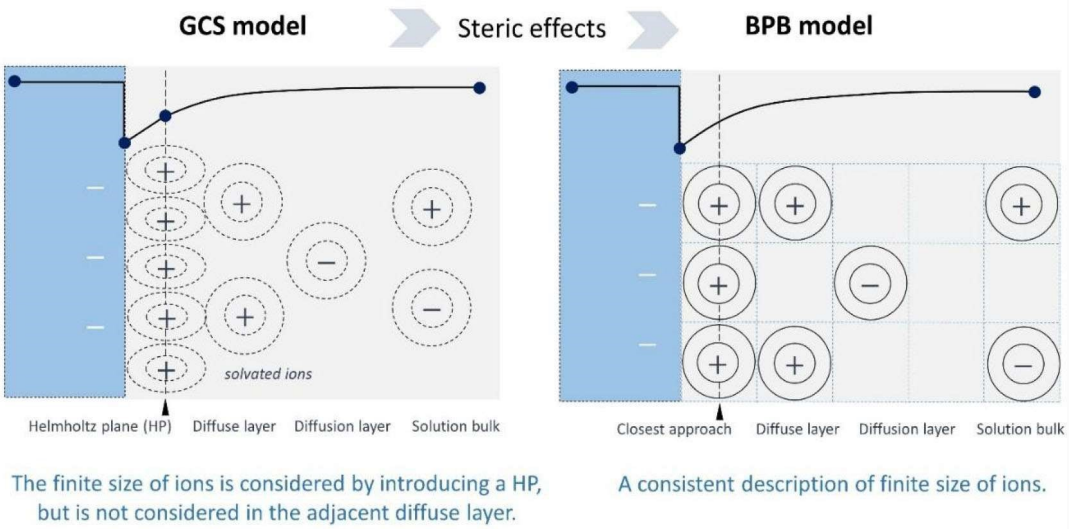

Figure 5 Schematic illustration of the comparison between the GCS model and the BPB model. For the GCS model, the number density of particles at the HP and in the diffuse layer can be infinite for the point charge assumption. Correspondingly, we depict ions with dotted lines in the GCS model, c.f. solid lines for ions of finite size in the BPB model. (color on line)

minimum at ϕ_{pzc}.

A simple calculation can illustrate the failure of the GCS model in extreme cases. According to Eq.(3), $c_i = c_i^b \exp(-z_i F\phi/RT)$, we obtain $c_i = 8.18 \times 10^{16}$ mol·m^{-3}, when $\phi = -1$ V, $z_i = 1$, $c_i^b = 1$ mol·m^{-3} and $T = 298$ K. Consequently, each cation occupies a volume of 2.03×10^{-35} cm^3. However, even for the smallest bare cation, H^+, the volume is approximately, $d_{H^+}{}^3 \approx (0.56\ \text{Å})^3 = 1.76 \times 10^{-25}$ cm^3 [45]. Thus, it is necessary to consider the finite size of ions in the diffuse layer.

3.2 Symmetric Bikerman Model

In 1942, Bikerman realized the limitations of neglecting ion size in the GCS model and developed a new model, called Bikerman-Poisson-Boltzmann (BPB) model, as shown in Figure 5[10, 46]. In contrast with the GCS model, the BPB model presents a consistent treatment of the finite size of ions both at the HP and in the diffuse layer.

The BPB model treats the electrolyte solution using the lattice-gas approach. Each ion occupies a volume of d_t^3, where d_t is the lattice size. The maximum particle number density is $n_t = d_t^{-3}$. The electrochemical potential for ion i reads,

$$\bar{\mu}_i = \mu_i^0 + z_i e_0 \phi + k_B T \ln \frac{d_t^3 n_i}{1 - d_t^3 \sum_i n_i} \tag{16}$$

where μ_i^0 is the chemical potential under standard conditions, e_0 the elementary charge, ϕ the electric potential referenced to that in the bulk solution, ϕ_S, k_B the Boltzmann constant, n_i the number density of ion i, $(1-d_t^3 \sum_i n_i)/d_t^3$ the number density of solvent molecules. For a monovalent electrolyte solution, we have $n_+^0 = n_-^0 = n^b$, with n^b the number density of total anions (cations) in the bulk solution. Under equilibrium conditions, the electrochemical potential for ion i is uniform in the whole EDL,

$$\bar{\mu}_i = \mu_i^0 + z_i e_0 \phi + k_B T \ln \frac{d_t^3 n_i}{1 - d_t^3 \sum_i n_i} = \mu_i^0 + k_B T \ln \frac{d_t^3 n^b}{1 - 2 d_t^3 n^b} \tag{17}$$

The number density of ion i is obtained as,

$$n_i = \frac{n^b \exp(-z_i e_0 \phi / k_B T)}{1 + 2v \sinh^2(z_i e_0 \phi / 2 k_B T)} \tag{18}$$

where the bulk volume fraction of solvated ions is $v = 2 d_t^3 n^b$. The GCS model assumes $v = 0$.

Combining Eq. (2) and Eq. (18), the BPB model is described as,

$$\nabla (\epsilon_s \nabla \phi) = \frac{2 n^b z_i e_0 \sinh(z_i e_0 \phi / k_B T)}{1 + 2v \sinh^2(z_i e_0 \phi / 2 k_B T)} \tag{19}$$

In a one dimensional case, the dimensionless form is,

$$\frac{\partial^2 U}{\partial X^2} = \frac{\sinh U}{1 + 2v \sinh^2(U/2)} \tag{20}$$

The surface charge density can be calculated as,

$$\sigma_M = -\int (n_+ - n_-) e_0 \, dx = -\epsilon_s \left(\frac{\partial \phi}{\partial x} \right)_{x = 0^+} \tag{21}$$

The 'bvp4c' function in Matlab is employed to solve Eq. (20) closed with the boundary conditions expressed in Eqs. (6) and (7). Figure 6 shows the typical results of the BPB model, including the spatial distributions of ϕ and the anion concentration, c_-, at a series of ϕ_M in (A) and (B), as well as the relationships between σ_M and C_{dl} with ϕ_M in (C) and (D). For the purpose of comparison, the results of the GCS model at $\phi_M - \phi_{pzc} = 0.7$ V are shown in the black solid lines. The distributions of ϕ and c_- calculated using the GCS model are steeper than those calculated using the BPB model. In Figure 6(B), a plateau forms when $\phi_M - \phi_{pzc} \geqslant 0.3$ V, signifying the natural formation of the Stern layer due to the overcrowding of counterions. Figures 6(C) and 6(D) display how σ_M and C_{dl} change with ϕ_M at three values of v. A larger v means either larger ions or higher concentrations or

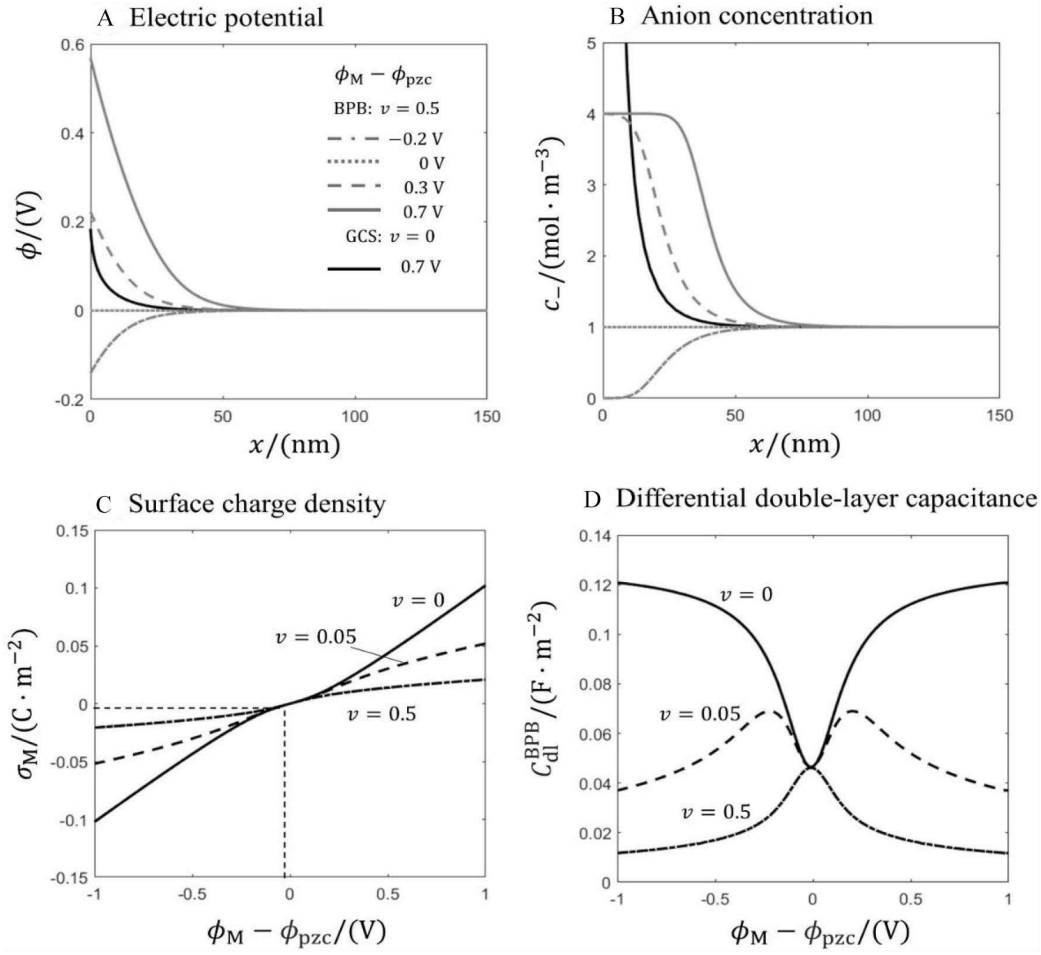

Figure 6 Typical results of the BPB model, including the spatial distributions of the electric potential and the anion concentration at a series of electrode potential in (A) and (B), and the relationships between (C) the surface charge density (D) the differential double-layer capacitance with the electrode potential. For the purpose of comparison, the results of the GCS model are shown in the black solid lines. The parameters for calculation are listed in Table 1. Matlab script of this model is provided in the supporting information. (color on line)

both. At larger v, the relationship between σ_M and ϕ_M is less steep, indicating smaller values of C_{dl}. Interestingly, the shape of C_{dl} changes from a camel shape with the minimum at ϕ_{pzc} to a bell shape with the maximum at ϕ_{pzc}. Kornyshev gives a critical value of v = 1/3 for the camel-to-bell transition[47].

3.3 Asymmetric Size Effect

With the asymmetric size effect, the electrochemical potential, Eq. (16), is rewritten as,

$$\bar{\mu}_i = \mu_i^{\ 0} + z_i e_0 \phi + k_B T \ln \frac{d_t^3 n_i}{1 - d_t^3 \sum_i \gamma_i n_i} \tag{22}$$

where γ_i is the size coefficient,

$$\gamma_i = \left(\frac{d_i}{d_t} \right)^3 \tag{23}$$

with d_i being the length of the cubic cell occupied by particle i, and d_t the reference size, usually taken as that of solvent molecules.

The number density for a monovalent electrolyte solution reads[48],

$$n_{\pm} = \frac{n^{b} e^{\mp U}}{1+\frac{v}{2}(\gamma_{+}e^{-U} + \gamma_{-}e^{U} - \gamma_{+} - \gamma_{-})} \tag{24}$$

To obtain Eq.(24), γ_+ and γ_- in the exponent are approximated as 1. Combining Eq.(2), the dimensionless form of the BPB equation in a one-dimensional case is,

$$\frac{\partial^2 U}{\partial X^2} = \frac{\sinh U}{1+\frac{v}{2}(\gamma_{+}e^{-U} + \gamma_{-}e^{U} - \gamma_{+} - \gamma_{-})} \tag{25}$$

Typical results of the asymmetric BPB model are presented in Figure 7, showing how σ_M and C_{dl} change with ϕ_M for the cases of different size coefficients. We set v = 0.05, and the size coefficient of cations, γ_+, or that of anions, γ_-, is equal to 1 or 3. At larger γ_i, the relationship between σ_M and ϕ_M is less steep, indicating smaller values of C_{dl}. γ_+ has bigger impact than γ_- as $\phi_M - \phi_{pzc} < 0$ because the concentration of cations dominates in this region due to the electrostatic interaction. γ_- plays an important role as $\phi_M - \phi_{pzc} > 0$.

4 Nonequilibrium Models

In this part we consider dynamics of the EDL brought out of equilibrium. We build nonequilibrium models by using a grand potential approach, considering the size asymmetry effects. The solvent polarization which leads to a field-dependent dielectric permittivity is considered in ref. [49], but is neglected in the following. Being grand-can-onical, the EDL exchanges electrons freely with the electrode and exchanges ions and solvent molecules freely with the bulk solution. Note that the EDL described here is not limited to a multiple of the Debye length, but could be extended to the bulk solution, because the diffuse layer and the diffusion layer are described by the same set of equations.

Under the conditions of constant electrochemical potential $\bar{\mu}_i$, constant T and a fixed volume V, the grand potential Ω of the EDL is written as,

$$\Omega = U - TS - \int \mathrm{d}V \sum_i \bar{\mu}_i n_i \tag{26}$$

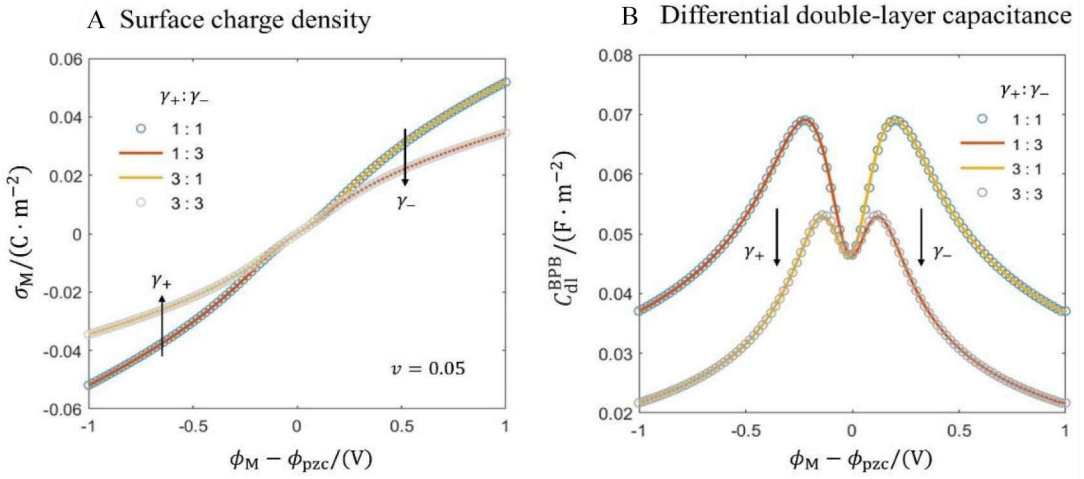

Figure 7 Typical results of the BPB model with the asymmetric size effect, including the relationships between (A) the surface charge density and (B) the differential double-layer capacitance with the electrode potential. The results of the symmetric BPB model are shown in the blue circles, as $\gamma_+ = \gamma_- = 1$. The results at $\gamma_+ = 1$ and $\gamma_- = 3$ are shown in the red solid lines, while the results at $\gamma_+ = 3$ and $\gamma_- = 1$ are shown in the yellow solid lines. The grey circles represent the results at $\gamma_+ = \gamma_- = 3$. The parameters for calculation are listed in Table 1. Matlab script of this model is provided in the supporting information. (color on line)

where U is the internal energy, S the entropy, $\bar{\mu}_i$ the electrochemical potential of particle i, n_i the number density of particle i, dV the volume unit.

There are multiple ions and solvent molecules in the electrolyte solution in general. Ions, denoted with a subscript α, have a charge number z_α and a number density n_α. There is a population of ions at (near) the transition state of the ion hopping process[50], denoted with a superscript $\neq$. Solvent molecules are denoted with a subscript s. These charged particles, namely, ions and solvent molecules at both ground and excited states, interact via coulombic forces among others. According to field theoretic studies of the coulombic fluid[51, 52], the internal energy U is expressed as,

$$U = \int \mathrm{d}V\left(-\frac{1}{2}\epsilon_\mathrm{s}(\nabla\phi)^2 + e_0\phi\sum(z_\alpha n_\alpha + z_{\alpha^\neq} n_{\alpha^\neq}) + \sum(n_\alpha H_\alpha + n_{\alpha^\neq}(H_\alpha + E_{a,\alpha^\neq}))\right) \tag{27}$$

The first two terms represent the electrostatic interactions, including the self-energy correction of the electric field, $-\frac{1}{2}\epsilon_\mathrm{s}(\nabla\phi)^2$, and the electrostatic free energies of the ions, $e_0\phi\sum z_\alpha n_\alpha$, and that of the transition-state ions, $e_0\phi\sum z_{\alpha^\neq} n_{\alpha^\neq}$. The last term accounts for many-body interactions other than the electrostatic interactions, with H_α being the internal energy except the electrostatic contribution, $E_{a,\alpha^\neq}$ the activation energy of ion hopping.

The total entropy S is calculated from the lattice-gas model[48],

$$S = \sum k_\mathrm{B}\ln P \tag{28}$$

where P is the number of ways arranging all the particles in the volume unit dV,

$$P = \frac{N_\mathrm{t}!}{\prod N_\alpha! N_\mathrm{s}! \prod N_{\alpha^\neq}!} \tag{29}$$

where $N_\alpha = n_\alpha \mathrm{d}V$, $N_\mathrm{s} = n_\mathrm{s}\mathrm{d}V$, and $N_{\alpha^\neq} = n_{\alpha^\neq}\mathrm{d}V$ are the particle numbers, and $N_\mathrm{t} = n_\mathrm{t}\mathrm{d}V$ is the total number of lattice cells in the volume unit, with n_t the number density.

The lattice cells are fully occupied without any vacancy, thus N_s is given by,

$$N_\mathrm{s} = \frac{N_\mathrm{t}}{\gamma_\mathrm{s}} - \sum\left(\frac{N_\alpha\gamma_\alpha}{\gamma_\mathrm{s}}\right) - \sum\left(\frac{N_{\alpha^\neq}\gamma_{\alpha^\neq}}{\gamma_\mathrm{s}}\right) \tag{30}$$

Note that there are several methods to treat size asymmetry in the lattice-gas model, as recently compared by Zhang and Huang[48]. What we have used in Eqs. (29) and (30) is Huang's treatment[53]. The basic idea is to effectively expand the number of total sites. However, the size asymmetry is not considered in the calculation of P expressed in Eq. (29). As shown by Zhang and Huang, this approach captures major phenomena of the asymmetric steric effects and avoids the artificial sequence effects[48].

Using the Stirling formula and taking the continuous limit (transforming the summation to a volume integration), we reformulate Eq. (28) as,

$$S = -\int \mathrm{d}V k_\mathrm{B}\left(\sum n_\alpha\ln\frac{n_\alpha}{n_\mathrm{t}} + n_\mathrm{s}\ln\frac{n_\mathrm{s}}{n_\mathrm{t}} + \sum n_{\alpha^\neq}\ln\frac{n_{\alpha^\neq}}{n_\mathrm{t}} + n_\mathrm{t} - \sum n_\alpha - n_\mathrm{s} - \sum n_{\alpha^\neq}\right) \tag{31}$$

Combining Eqs. (26), (27), and (31), we rewrite the grand potential as a volume integration of a volumetric grand potential,

$$\Omega = \int f\mathrm{d}V \tag{32}$$

with the volumetric grand potential f given by,

$$f = -\frac{1}{2}\epsilon_\mathrm{s}(\nabla\phi)^2 + e_0\phi\sum(z_\alpha n_\alpha + z_{\alpha^\neq} n_{\alpha^\neq}) + \sum(n_\alpha H_\alpha + n_{\alpha^\neq}(H_\alpha + E_{a,\alpha^\neq})) +$$

$$\frac{1}{\beta}\left(\sum n_\alpha\ln\frac{n_\alpha}{n_\mathrm{t}} + n_\mathrm{s}\ln\frac{n_\mathrm{s}}{n_\mathrm{t}} + \sum n_{\alpha^\neq}\ln\frac{n_{\alpha^\neq}}{n_\mathrm{t}} + n_\mathrm{t} - \sum n_\alpha - n_\mathrm{s} - \sum n_{\alpha^\neq}\right) - \left(\sum\bar{\mu}_\alpha n_\alpha + \bar{\mu}_\mathrm{s} n_\mathrm{s} + \sum\bar{\mu}_{\alpha^\neq} n_{\alpha^\neq}\right) \tag{33}$$

Using the Euler-Lagrange equation,

$$\frac{\partial f}{\partial X} - \nabla\left(\frac{\partial f}{\partial(\nabla X)}\right) = 0 \tag{34}$$

in terms of $X = \phi$, we obtain the Poisson equation,

$$\frac{\partial}{\partial x}\left(\epsilon_s \frac{\partial \phi}{\partial x}\right) = -e_0 \sum (z_\alpha n_\alpha + z_{\alpha^{\neq}} n_{\alpha^{\neq}}) \tag{35}$$

When applying the Euler-Lagrange equation in terms of $X = n_\alpha$, we must take notice of the relation that $n_s = n_t/\gamma_s - \sum n_\alpha\gamma_\alpha/\gamma_s - \sum n_{\alpha^{\neq}}\gamma_{\alpha^{\neq}}/\gamma_s$ is also a function of n_α. Therefore, adding an ion α will simultaneously reduce γ_α/γ_s solvent molecules. The consideration leads to,

$$z_\alpha e_0\phi + H_\alpha + \frac{1}{\beta}\left(\ln\frac{n_\alpha}{n_t} - \frac{\gamma_\alpha}{\gamma_s}\ln\frac{n_s}{n_t}\right) - \bar{\mu}_\alpha + \frac{\gamma_\alpha}{\gamma_s}\bar{\mu}_s = 0 \tag{36}$$

from which we define the electrochemical potential of the ion-solvent pair,

$$\bar{\mu}_{\alpha\text{-s}} = \bar{\mu}_\alpha - \frac{\gamma_\alpha}{\gamma_s}\bar{\mu}_S \tag{37}$$

with the electrochemical potential of solvent molecules expressed as,

$$\bar{\mu}_s = \frac{1}{\beta}\ln\frac{n_s}{n_t} \tag{38}$$

and the electrochemical potential of ions α as,

$$\bar{\mu}_\alpha = H_\alpha + z_\alpha e_0\phi + \frac{1}{\beta}\ln\frac{n_\alpha}{n_t} \tag{39}$$

When the fictitious lattice cells are occupied exclusively by ions α, namely, $n_t = n_\alpha$, the chemical potential turns to the standard chemical potential of ions α, denoted as μ_α^0,

$$\mu_\alpha^0 = H_\alpha \tag{40}$$

Applying the Euler-Lagrange equation in terms of $X = n_{\alpha^{\neq}}$, we obtain the standard chemical potential of transition-state ions $\alpha^{\neq}$,

$$\mu_{\alpha^{\neq}}^0 = H_\alpha + E_{a\alpha^{\neq}} \tag{41}$$

Although the transition-state ions are explicitly included in the grand-canonical potential, we will make the approximate that $n_{\alpha^{\neq}} \ll n_\alpha$ in the following.

According to the Fick's second law, the continuity equation for particle α in the i^{th} cubic cell is written as,

$$\frac{\partial n_\alpha^i}{\partial t} = -\frac{\partial J_\alpha^i}{\partial x} \tag{42}$$

where J_α^i is the flow flux of particle α cross the i^{th} cubic cell, the interface between the i^{th} cubic cell and the $(i+1)^{th}$ cubic cell,

$$J_\alpha^i = J_\alpha^{i\to i+1} - J_\alpha^{i+1\to i} = \frac{1}{d_t^2}\left(k_\alpha^{i\to i+1}\frac{n_\alpha^i}{n_t}\frac{n_s^{i+1}}{n_t} - k_\alpha^{i+1\to i}\frac{n_\alpha^{i+1}}{n_t}\frac{n_s^i}{n_t}\right) \tag{43}$$

Eq.(43) means that the ion transport process is pictured as an ion-solvent exchange reaction, which has been proposed earlier to describe ion transport in solid and concentrated electrolytes[50, 54], where $k_\alpha^{i\to i+1}$ and $k_\alpha^{i+1\to i}$ represent the forward and backward rates of ion hopping from the i^{th} to $(i+1)^{th}$ cubic cell, respectively. According to transition-state theory and using the Brønsted-Evans-Polanyi (BEP) relationship to associate the activation barrier and the Gibbs free energy change, we write $k_\alpha^{i\to i+1}$ as,

$$k_\alpha^{i\to i+1} = k_\alpha^0\exp\left(-\frac{\beta}{2}(\bar{\mu}_{\alpha\text{-s}}^{i+1} - \bar{\mu}_{\alpha\text{-s}}^i)\right) = k_\alpha^0\exp\left(-\frac{\beta}{2}\nabla\bar{\mu}_{\alpha\text{-s}}d_t\right) \tag{44}$$

and $k_\alpha^{i+1\to i}$ as,

$$k_\alpha^{i+1\to i} = k_\alpha^0\exp\left(-\frac{\beta}{2}(\bar{\mu}_{\alpha\text{-s}}^i - \bar{\mu}_{\alpha\text{-s}}^{i+1})\right) = k_\alpha^0\exp\left(\frac{\beta}{2}\nabla\bar{\mu}_{\alpha\text{-s}}d_t\right) \tag{45}$$

where the standard rate constant k_α^0 is expressed as,

$$k_\alpha^0 = \frac{1}{2\tau_{\alpha 0}}\exp(-\beta(\mu_{\alpha^{\neq}}^0 - \mu_\alpha^0)) = \frac{1}{2\tau_{\alpha 0}}\exp(-\beta E_{a\alpha^{\neq}}) \tag{46}$$

with $\tau_{\alpha,0}$ being the time constant of the hopping process. The 1/2 here indicates that ions at the transition state are equally likely to go forward to the new state and backward to the original state.

Substituting Eqs. (44), (45) and (46) into (43), we rewrite the flux as,

$$J_\alpha = -\frac{2D_\alpha}{d_t^4}\sinh\left(\frac{\beta}{2}\nabla\bar{\mu}_{\alpha\text{-}s}d_t\right)\frac{n_\alpha}{n_t}\frac{n_s}{n_t} \tag{47}$$

where D_α is the diffusion coefficient,

$$D_\alpha = \frac{d_t^2}{2\tau_{\alpha 0}}\exp(-\beta E_{a\alpha^{\neq}}) \tag{48}$$

In the near-equilibrium regime, $\sinh(\beta d_t \nabla\bar{\mu}_{\alpha\text{-}s}/2) \approx \beta d_t \nabla\bar{\mu}_{\alpha\text{-}s}/2$, Eq. (47) can be approximated to,

$$J_\alpha = -D_\alpha\beta\frac{n_\alpha n_s}{n_t}\nabla\bar{\mu}_{\alpha\text{-}s} \tag{49}$$

where $\nabla\bar{\mu}_{\alpha\text{-}s}$ is expanded as,

$$\nabla\bar{\mu}_{\alpha\text{-}s} = \frac{1}{\beta n_\alpha}\frac{\partial n_\alpha}{\partial x} + \frac{1}{\beta n_s}\frac{\gamma_\alpha}{\gamma_s}\sum_{i\neq s}\frac{\gamma_i}{\gamma_s}\frac{\partial n_i}{\partial x} + z_\alpha e_0\frac{\partial\phi}{\partial x} \tag{50}$$

Combining Eqs. (42), (49) and (50), we obtain a modified Nernst-Planck equation,

$$\frac{\partial n_\alpha}{\partial t} = \frac{\partial}{\partial x}\left(D_\alpha\frac{n_s}{n_t}\frac{\partial n_\alpha}{\partial x} + D_\alpha\frac{n_\alpha}{n_t}\frac{\gamma_\alpha}{\gamma_s}\sum_{i\neq s}\frac{\gamma_i}{\gamma_s}\frac{\partial n_i}{\partial x} + D_\alpha\beta\frac{n_\alpha n_s}{n_t}z_\alpha e_0\frac{\partial\phi}{\partial x}\right) \tag{51}$$

The modified Poisson-Nernst-Planck (PNP) equations in Eq. (35) and Eq. (51) constitute the continuum model for multicomponent mass transport in electrolyte solution, which is derived from the grand potential being a functional of the electric potential and the particle number densities.

The boundary conditions and the initial conditions are necessary for solving the PNP equation, a set of partial differential equations. The boundary conditions are commonly divided into three types, Dirichlet, Neumann and Robin. Dirichlet boundary conditions specify the variable value on the boundary, for example, $y = y_0$ at $x = x_0$. Neumann boundary conditions specify the derivative of the variable, for example, $\frac{\partial y}{\partial x} = \alpha$ at $x = x_0$. Robin boundary conditions are a combination of Dirichlet and Neumann boundary conditions, for example, $y - \frac{\partial y}{\partial x} = 0$ at $x = x_0$.

The reaction plane, designated as the coordinate origin, $x = 0$, is the left boundary of which conditions are,

$$J_\alpha = m_\alpha\frac{j}{me_0} \tag{52}$$

$$\phi(0, t) = \phi_M - \phi_{pzc} + \frac{\partial\phi}{\partial x}(0, t)\delta_{HP}\frac{\epsilon_s}{\epsilon_{HP}} \tag{53}$$

where j represents the current density of the overall reaction, m is the number of transferred electrons in the overall reaction, m_α is the stoichiometric number of the particle α in the overall reaction. If particle α does not participate in the reaction, we use $m_\alpha = 0$. Eq. (53) shows the electric potential at the HP calculated from the electrode side, which is the same as Eq. (8). Eq. (52) is a Neumann boundary condition, while Eq. (53) is a Robin boundary condition.

The bulk solution is the right boundary, $x = x_r$, with the following natural boundary conditions,

$$n_\alpha(x_r, t) = n_\alpha^b \tag{54}$$

$$\phi(x_r,t) = 0 \tag{55}$$

which are the Dirichlet boundary conditions, where n_α^b is the number density of particle α in the bulk solution.

At $t = 0$, the initial conditions are shown as,

$$n_\alpha(x,0) = n_\alpha^b \tag{56}$$

$$\phi(x,0) = 0 \tag{57}$$

We consider a proton-coupled electron transfer reaction, $A + H^+ + e^- \leftrightarrow B$, occurring at the HP, with A and B being neutral species. The current density of the reaction, j, is described by the Frumkin-Butler-Volmer (FBV) equation[55],

$$j = e_0 n_M k_{00} \left(\frac{c_{B,HP}}{c_B^0} \exp\left(\frac{\alpha e_0 \eta}{k_B T} \right) - \frac{c_{A,HP}}{c_A^0} \frac{c_{H^+,HP}}{c_{H^+}^0} \exp\left(- \frac{(1-\alpha) e_0 \eta}{k_B T} \right) \right) \tag{58}$$

where n_M is the areal number density of the electrode. For example, n_M is calculated by $(\sqrt{3}\, a_M^2)^{-1}$ for M(111) with the lattice constant a_M. The pre-exponential factor k_{00} is equal to $\frac{k_B T}{h} \exp\left(- \frac{\Delta G_a^{00}}{k_B T} \right)$, with h being the Planck constant, ΔG_a^{00} the activation energy of the reaction at standard equilibrium state. α is the charge transfer coefficient, taken as 0.5. $c_{B,HP}$, $c_{A,HP}$ and $c_{H^+,HP}$ are the concentrations of B, A and H^+ at the HP, respectively. c_B^0, c_A^0 and $c_{H^+}^0$ are the concentrations of B, A and H^+ under standard conditions, respectively. η is the overpotential, defined as,

$$\eta = \phi_M - \phi_{HP} - E^{00} \tag{59}$$

where E^{00} is the equilibrium potential of the reaction under standard conditions, calculated by $E^{00} = -\Delta G^0/e_0$, with ΔG^0 being the Gibbs free energy under standard conditions.

We numerically solve the model using the built-in partial differential equations solver, pdepe function, in Matlab, with the parameters listed in Table 1. Matlab script of this model is provided in the supporting information.

The typical results of the PNP equation are shown in Figure 8, including the steady current density, j, as a function with ϕ_M, and the distributions of the concentration of A, c_A, at 0.1 s, 1 s and 5 s at 0.4 V_{SHE}. The spatial range of the EDL is 100 μm, and the time duration is 5 s. The steady current density is taken at 5 s. As $\phi_M > E^{00}$, the oxidation reaction occurs and B is consumed. The current density increases near exponentially in the low overpotential region and transitions to the diffusion limiting region when $\phi_M > 0.7$ V_{SHE}, caused by the low concentration of B at the HP. When $\phi_M < E^{00}$, the reduction reaction occurs. As the electric potential decreases, the current density increases and reaches the diffusion limiting current, which is limited by the low concentration of A at the HP. From Figure 8(B), we see as the reduction reaction occurs, the concentration of A at the HP is lower than that in the bulk solution, and decreases as the reaction continues. At 5 s, c_A becomes almost linear and reaches almost zero at the HP, signifying diffusion limiting effects.

Then we apply some approximations to reduce the modified PNP equation back to the classical PNP equation. Firstly, under the assumption $n_{\alpha^{\neq}} \ll n_\alpha$, Eq. (35) is simplified as,

$$\frac{\partial}{\partial x}\left(\epsilon_s \frac{\partial \phi}{\partial x} \right) = - e_0 \sum z_\alpha n_\alpha \tag{60}$$

As for the modified Nernst-Planck equation, neglect of the asymmetric steric effects, that is, $\gamma_i = 1$, simplifies Eq. (51) to,

$$\frac{\partial n_\alpha}{\partial t} = \frac{\partial}{\partial x}\left(D_\alpha \frac{n_s}{n_t} \frac{\partial n_\alpha}{\partial x} + D_\alpha \frac{n_\alpha}{n_t} \sum_{i \neq s} \frac{\partial n_i}{\partial x} + D_\alpha \beta \frac{n_\alpha n_s}{n_t} z_\alpha e_0 \frac{\partial \phi}{\partial x} \right) \tag{61}$$

Furthermore, if the electrolyte is sufficiently dilute, that is, $n_\alpha \ll n_t$, and $n_t \approx n_s$, the expression is returned back to the classical Nernst-Planck equation,

$$\frac{\partial n_\alpha}{\partial t} = \frac{\partial}{\partial x}\left(D_\alpha \frac{\partial n_\alpha}{\partial x} + D_\alpha \beta n_\alpha z_\alpha e_0 \frac{\partial \phi}{\partial x} \right) \tag{62}$$

Table 1 List of the Model Parameters

Symbol (unit)	Value	Physical significance	Note
Constants			
k_B(J·K^{-1})	1.381 × 10^{-23}	Boltzmann constant	
T(K)	298.15	Absolute temperature	
h(J·s)	6.626 × 10^{-34}	Planck constant	
e_0(C)	1.602 × 10^{-19}	Elementary charge	
N_A(mol^{-1})	6.022 × 10^{23}	Avogadro constant	
ϵ_0(F·m^{-1})	8.854 × 10^{-12}	Vacuum permittivity	
F(C·mol^{-1})	96485	Faraday constant	
R(J·K^{-1}·mol^{-1})	8.314	Gas constant	
Solution properties			
ϵ_{HP}(F·m^{-1})	$6\epsilon_0$	Dielectric permittivity of the space between the electrode and the HP	Ref [56]
ϵ_s(F·m^{-1})	$78.5\epsilon_0$	Bulk dielectric permittivity of the water solvent medium	
δ_{HP}(nm)	0.4125	Distance from the electrode to the HP, calculated by 1.5 d_{H_2O} with the diameter of water d_{H_2O} = 0.275 nm.	
D(m^2·s^{-1})	1 × 10^{-9}	Diffusion coefficient	
c^b(mol·m^{-3})	1	Concentration of total cations (anions) in the bulk solution	
c_A^0,c_B^0,$c_{H^+}^0$(mol·m^{-3})	1	Concentrations of B, A and H^+ under standard conditions	
Electrode properties			
ϕ_{pzc}(V_{SHE})	0.3	Potential of zero charge	Estimated
a_M(Å)	3.5	Lattice constant of the electrode	Estimated
n_M(m^{-2})	4.713 × 10^{18}	Areal number density of M(111), calculated by $(\sqrt{3}\,a_M^2)^{-1}$	
Reaction properties			
E^{00}(V_{SHE})	0.6	Equilibrium potential of the reaction at standard state	Estimated
ΔG_a^{00}(eV)	0.4	Activation energy of the reaction at standard equilibrium state	Estimated

At equilibrium state, that is $J_\alpha = 0$, Eq. (62) turns into Eq. (3), the Boltzmann equation. Similarly, when $J_\alpha = 0$, Eq. (61) turns into Eq. (18), the equation adopted in the symmetric BPB model. Eq. (51) turns into Eq. (24), the equation used in the asymmetric BPB model.

5 AC Impedance Models

Electrochemical impedance spectroscopy (EIS) is an *in-situ*, non-invasive characterization tool that can separate multiple physicochemical processes spanning a wide frequency range. In most cases, the EIS of an EDL is analyzed using the electrical circuit model (ECM) as shown in Figure 9. In fact, as to be discussed in the next paragraph, the ECM has a very clear physical meaning. However, it is not rigorous, theoretically. Instead, it is based on several assumptions which may become invalid in some cases. Therefore, it is of general importance to derive the impedance response of the EDL that is described using the PNP theory—the 'first-principles' of continuum modelling of the EDL. We recommend the readers to follow the derivation with paper and pencil. This way, you will grasp the process of building a physical impedance model, acquire the basic mathematical tools,

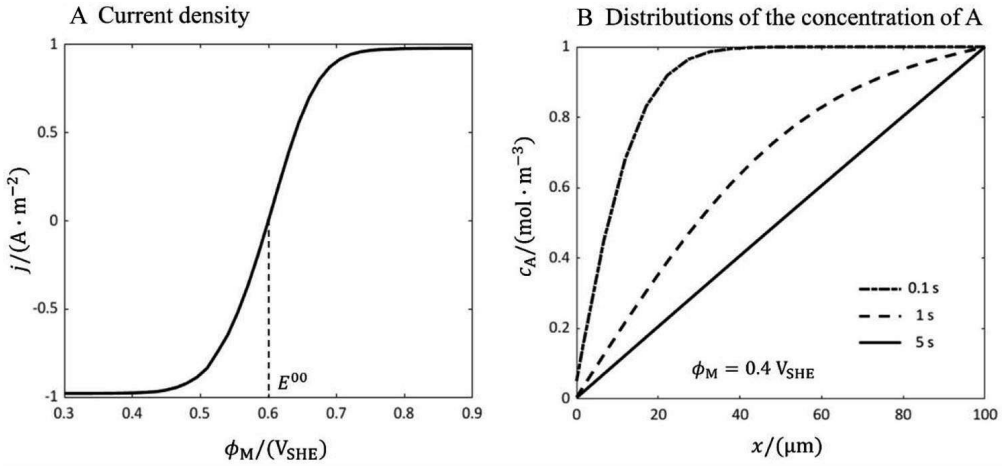

Figure 8 Typical results of the PNP theory, including the current density varying with the electrode potential, and the distributions of the concentration of A at 0.1 s, 1 s and 5 s at 0.4 V_{SHE}. The spatial range for calculation is 100 μm from the HP, and the time duration for calculation is 5 s. The parameters for calculation are listed in Table 1. Matlab script of this model is provided in the supporting information.

and appreciate the beauty of physicochemical modelling.

There are usually three physicochemical processes in the EDL: double-layer charging, charge transfer reactions, and diffusion. The double-layer charging involves redistribution of ions in the EDL, namely, change of the net charge stored in the EDL, under the control of the electric potential. As the EDL is usually only a few nanometers thick, ion transport in the EDL is often considered to be completed immediately. Therefore, charging the EDL is equivalent to charging an interfacial capacitance C_{dl}. As for the charge transfer reactions, it takes less than 1 ps for an electron to transfer between the electrode and the reactant in solution phase. Consequently, we can safely assume that the reaction current flows immediately when a potential difference is imposed. In other words, the current-electric potential relation of the charge transfer reaction is equivalent to that of a resistance R_{ct}. These two processes are in parallel because they are controlled by the same potential difference, and the total current is the sum of the double-layer charging part and the charge transfer reaction part. That is why the C_{dl} and R_{ct} are in parallel in Figure 9.

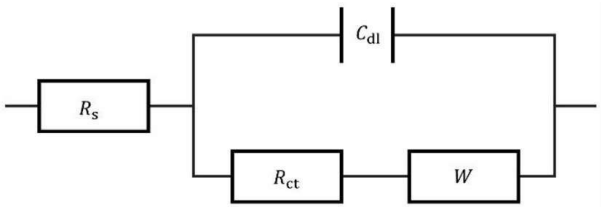

Figure 9 ECM in the electrochemical system. C_{dl} is an interfacial capacitance, associated with the double-layer charging process, R_{ct} is a resistance, associated with the charge transfer reactions process, W describes the diffusion of species involved in the charge transfer reactions, R_s is the electrolyte solution resistance, associated with the migration process in the bulk solution.

The W element in Figure 9 represents the diffusion of species involved in the charge transfer reactions in the electrolyte solution. The elements W and R_{ct} are in series because the transport process precedes/succeeds the charge transfer reactions. Conscious readers may have noticed a logic flaw: did not we consider ion transport in the EDL twice (one time in C_{dl}, and the other time in W)? There is another puzzle related to it. Given the fact that ion transport in the EDL and that in the diffusion layer are the same physical process, why do we need two elements? Why are C_{dl} and W located in different branches in the ECM? The way to resolve these puzzles has to be found via rigorous physicochemical modelling.

Before entering into physics-based impedance modelling, the definition of EIS and the fundamental

mathematical tool—Fourier transform—will be introduced. Then, we will work on calculating the impedance response of a basic ECM to express the working mechanism of Fourier transform. Readers may find that EIS is more than a specific kind of classical electrochemical techniques. It provides a powerful mathematical physics approach to solve the electrochemical problems and represents a different look at electrochemical problems.

5.1 Basics of EIS

In this section, we introduce concisely the basics of EIS, including the Fourier transform and the example of a simple electrical circuit.

5.1.1 Fourier transform

The Fourier transform of a function $f(t)$ is,

$$F(\omega) = \mathcal{F}(f(t)) = \int_{-\infty}^{\infty} f(t)\exp(-j\omega t)\mathrm{d}t \tag{63}$$

which transforms a time-domain signal $f(t)$ into a frequency-domain signal $F(\omega)$. The inverse Fourier transform is,

$$f(t) = \mathcal{F}^{-1}(F(\omega)) = \frac{1}{2\pi}\int_{-\infty}^{\infty} F(\omega)\exp(j\omega t)\mathrm{d}\omega \tag{64}$$

derived from Eq.(63) as follows,

$$F(\omega) = \int_{-\infty}^{\infty} f(t)\exp(-j\omega t)\mathrm{d}t = \frac{1}{2\pi}\int_{-\infty}^{\infty}\int_{-\infty}^{\infty} F(\omega')\exp(j\omega' t)\mathrm{d}\omega\exp(-j\omega t)\mathrm{d}t =$$

$$\frac{1}{2\pi}\int_{-\infty}^{\infty} F(\omega')\left(\int_{-\infty}^{\infty}\exp(-j(\omega-\omega')t)\mathrm{d}t\right)\mathrm{d}\omega = \int_{-\infty}^{\infty} F(\omega')\delta(\omega-\omega')\mathrm{d}\omega = F(\omega) \tag{65}$$

where we have used the Dirac's delta function $\delta(\omega-\omega') = \frac{1}{2\pi}\int_{-\infty}^{\infty}\exp(-j(\omega-\omega')t)\mathrm{d}t$.

Electrochemical processes are usually described by ordinary or partial differential equations. Therefore, the Fourier transform of the n^{th} derivative of a function is useful,

$$\mathcal{F}\left(\frac{\mathrm{d}^n f(t)}{\mathrm{d}t^n}\right) = (j\omega)^n F(\omega) \tag{66}$$

given that $f^{(n-1)}(t) = 0$ at the initial state.

We prove for the case $n = 1$,

$$\mathcal{F}\left(\frac{\mathrm{d}f(t)}{\mathrm{d}t}\right) = \int_{-\infty}^{\infty} f'(t)\exp(-j\omega t)\mathrm{d}t = f(t)\exp(-j\omega t)\Big|_{-\infty}^{\infty} + j\omega\int_{-\infty}^{\infty} f(t)\exp(-j\omega t)\mathrm{d}t = j\omega F(\omega) \tag{67}$$

where we use the natural boundary conditions, $f(\infty) = f(-\infty) = 0$. The case of other orders can be proved by repeating the manipulation of Eq.(67).

Another often-used property of Fourier transform is the convolution theorem,

$$\mathcal{F}(f(t)*g(t)) = F(\omega)G(\omega) \tag{68}$$

where the sign "*" denotes the convolution operator defined as $f(t)*g(t) = \int_{-\infty}^{\infty} f(\tau)g(t-\tau)\mathrm{d}\tau$, $F(\omega)$ and $G(\omega)$ denote the Fourier transform of $f(t)$ and $g(t)$, respectively. Eq. (68) is proved as follows,

$$\mathcal{F}(f(t)*g(t)) = \int_{-\infty}^{\infty}\int_{-\infty}^{\infty} f(\tau)g(t-\tau)\mathrm{d}\tau\exp(-j\omega t)\mathrm{d}t = \int_{-\infty}^{\infty}\int_{-\infty}^{\infty} f(\tau)e^{-j\omega t}g(t-\tau)e^{-j\omega(t-\tau)}\mathrm{d}\tau\mathrm{d}t$$

$$= \int_{-\infty}^{\infty} f(\tau)e^{-j\omega t}\left(\int_{-\infty}^{\infty} g(t-\tau)e^{-j\omega(t-\tau)}\mathrm{d}t\right)\mathrm{d}\tau = F(\omega)G(\omega) \tag{69}$$

5.1.2 Definition of Impedance

For any electrochemical system at stationary states, we apply an arbitrary current or electric potential excitation of small magnitude to ensure the linearity requirement, and obtain corresponding electric potential or current response. The electrochemical impedance is defined as the ratio of the Fourier transform of the potential to that of the current, that is,

$$Z(\omega) = \frac{\mathcal{F}(V(t))}{\mathcal{F}(i(t))} \tag{70}$$

A simple ECM is shown in Figure 10(A), which consists of two resistors and one capacitor. The total electric potential of this circuit is,

$$V_{tot}(t) = V_1(t) + V_2(t) \tag{71}$$

where

$$V_1(t) = R_0 i(t),\ i(t) = \frac{V_2(t)}{R} + C\frac{\mathrm{d}V_2(t)}{\mathrm{d}t} \tag{72}$$

Applying Fourier transform into Eqs. (71) and (72), we obtain,

$$\mathcal{F}(V_{tot}(t)) = \mathcal{F}(V_1(t)) + \mathcal{F}(V_2(t)) \tag{73}$$

$$\mathcal{F}(V_1(t)) = R_0\mathcal{F}(i(t)),\ \mathcal{F}(i(t)) = \frac{\mathcal{F}(V_2(t))}{R} + j\omega C\mathcal{F}(V_2(t)). \tag{74}$$

Combining Eqs. (70) and (74), the electrochemical impedance reads,

$$Z = \frac{\mathcal{F}(V_{tot}(t))}{\mathcal{F}(i(t))} = R_0 + \frac{R}{1+j\omega RC} \tag{75}$$

The real part, $Z'(\omega)$, and the imaginary part, $Z''(\omega)$, of Eq. (75) are,

$$Z'(\omega) = R_0 + R\frac{1}{1+(\omega\tau)^2} \tag{76}$$

$$Z''(\omega) = -R\frac{\omega\tau}{1+(\omega\tau)^2} \tag{77}$$

where $\tau = RC$ is the time constant of this circuit. The amplitude and phase angle of this impedance are,

$$|Z| = \sqrt{(Z')^2+(Z'')^2} = \sqrt{R_0^2 + \frac{R^2 + 2RR_0}{1+(\omega\tau)^2}} \tag{78}$$

$$\varphi = \operatorname{arctanh}\left(\frac{Z''}{Z'}\right) = -\operatorname{arctanh}\left(\frac{R\omega\tau}{R + R_0(1+(\omega\tau)^2)}\right) \tag{79}$$

Figure 10(B) shows the EIS of the $R_0(R//C)$ circuit in the Nyquist plot, which is a perfect semi-circle. The diameter of the semi-circle is equal to R and the high-frequency intercept on the horizontal axis is equal to R_0. We can also represent the EIS in the Bode plots in Figures 10(C) and 10(D). The relationship between the impedance amplitude and the frequency is shown in Figure 10(C). At very low frequencies, the amplitude of impedance is equal to $R + R_0$. At very high frequencies, the amplitude of impedance approaches R_0. Figure 10(D) shows how the phase angle varies with frequency. There is only a characteristic frequency at $1/RC$ which corresponds to the peak in the Nyquist plot. Notably, the peak frequency in the Bode plot deviates from $1/RC$[57].

5.1.3 Perturbation Analysis

Considering a dilute, symmetrical and covalent electrolyte solution, we apply a potential perturbation to the system,

$$U_M = U_M^0 + \widetilde{U}_M e^{j\omega^{nd}\tau} \tag{80}$$

where U_M is the dimensionless electrode potential, the superscript "0" denotes the stationary electrode potential, the sign "~" denotes the magnitude of the perturbation potential and ω^{nd} is the dimensionless angular frequency referenced to D/λ_D^2. When the perturbation is sufficiently weak ($\widetilde{\phi}_M < 25$ mV, or $\widetilde{U}_M < 1$), the linear response approximation is valid. Then, all system variables are decomposed into stationary parts and perturbation parts of the same frequency, namely,

$$C_+ = C_+^0 + \widetilde{C}_+ e^{j\omega^{nd}\tau} \tag{81}$$

$$C_- = C_-^0 + \widetilde{C}_- e^{j\omega^{nd}\tau} \tag{82}$$

$$U = U^0 + \widetilde{U} e^{j\omega^{nd}\tau} \tag{83}$$

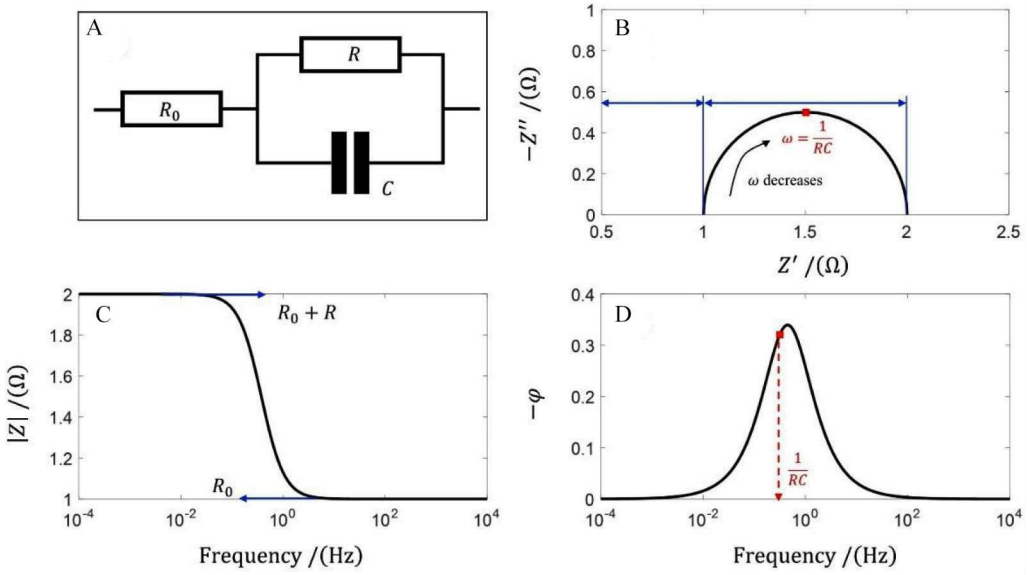

Figure 10 (A) A simple RC electrical circuit; (B) The Nyquist plot; (C) The Bode plot of amplitude; (D) The Bode plot of phase angle. The parameters used for calculation are as follows, $R_0 = R = 1\ \Omega$, $C = 0.5$ F, and the frequency range: 1×10^{-4} Hz to 1×10^{4} Hz. Matlab script of this model is provided in the supporting information. (color on line)

Substituting Eqs. (81)-(83) into the PNP equation, and omitting the stationary and high-order parts, we obtain,

$$j\omega^{nd}\widetilde{C}_+ = \frac{\partial^2\widetilde{C}_+}{\partial X^2} + \frac{\partial}{\partial X}\left(C_+^{\,0}\frac{\partial\widetilde{U}}{\partial X} + \widetilde{C}_+\frac{\partial U^0}{\partial X}\right) \tag{84}$$

$$j\omega^{nd}\widetilde{C}_- = \frac{\partial^2\widetilde{C}_-}{\partial X^2} - \frac{\partial}{\partial X}\left(C_-^{\,0}\frac{\partial\widetilde{U}}{\partial X} + \widetilde{C}_-\frac{\partial U^0}{\partial X}\right) \tag{85}$$

$$\frac{\partial^2\widetilde{U}}{\partial X^2} = \frac{1}{2}(\widetilde{C}_- - \widetilde{C}_+). \tag{86}$$

Usually, $C_+^{\,0}$, $C_-^{\,0}$ and U^0 are X-varying, making it difficult to solve Eqs. (84)-(86) analytically. Nevertheless, at the pzc, we have, $C_+^{\,0} = C_-^{\,0} = 1$ and $U^0 = 0$. Therefore, Eqs. (84) and (85) are reduced to,

$$j\omega^{nd}\widetilde{C}_+ = \frac{\partial^2\widetilde{C}_+}{\partial X^2} + \frac{\partial^2\widetilde{U}}{\partial X^2} \tag{87}$$

$$j\omega^{nd}\widetilde{C}_- = \frac{\partial^2\widetilde{C}_-}{\partial X^2} - \frac{\partial^2\widetilde{U}}{\partial X^2} \tag{88}$$

Substituting Eq. (86) into Eqs (87) and (88) leads,

$$\frac{\partial^2\widetilde{C}_+}{\partial X^2} = (j\omega^{nd} + \frac{1}{2})\widetilde{C}_+ - \frac{1}{2}\widetilde{C}_- \tag{89}$$

$$\frac{\partial^2\widetilde{C}_-}{\partial X^2} = -\frac{1}{2}\widetilde{C}_+ + (j\omega^{nd} + \frac{1}{2})\widetilde{C}_- \tag{90}$$

Two equations above can be rewritten into a matrix form,

$$\frac{\partial^2}{\partial X^2}\mathbf{x} = \mathbf{A}\mathbf{x} \tag{91}$$

$$\mathbf{A} = \begin{bmatrix} \Theta_1 & \Theta_2 \\ \Theta_2 & \Theta_1 \end{bmatrix} \tag{92}$$

$$\mathbf{x} = [\widetilde{C}_+, \widetilde{C}_-]^T \tag{93}$$

$$\mathbf{\Theta}_1 = (j\omega^{nd} + \frac{1}{2}) \tag{94}$$

$$\mathbf{\Theta}_2 = -\frac{1}{2}. \tag{95}$$

The eigenvalues, λ_1 and λ_2, and eigenvectors, V_1 and V_2, of matrix **A** are,

$$\lambda_1 = \mathbf{\Theta}_1 - \mathbf{\Theta}_2 \tag{96}$$

$$\lambda_2 = \mathbf{\Theta}_1 + \mathbf{\Theta}_2 \tag{97}$$

$$V_1 = [-1,1]^T \tag{98}$$

$$V_2 = [1,1]^T. \tag{99}$$

Introducing two matrixes **P** and **H**, and a vector **y**,

$$\mathbf{P} = \begin{bmatrix} -1 & 1 \\ 1 & 1 \end{bmatrix} \tag{100}$$

$$\mathbf{H} = \begin{bmatrix} \lambda_1 & 0 \\ 0 & \lambda_2 \end{bmatrix} \tag{101}$$

$$\mathbf{y} = \mathbf{P}^{-1}\mathbf{x} \tag{102}$$

then we substitute the vector **x** with **y** and using the equality, $\mathbf{P}^{-1}\mathbf{AP} = \mathbf{H}$, transforming Eq. (91) into,

$$\frac{\partial^2}{\partial X^2}\,\mathbf{y} = \mathbf{H}\mathbf{y}. \tag{103}$$

Notice that **H** is a diagonal matrix, implying that the two elements of vector **y**, y_1 and y_2, can be solved separately,

$$y_1 = \alpha_1 \sinh(\sqrt{\lambda_1}\, X) + \alpha_2 \cosh(\sqrt{\lambda_1}\, X) \tag{104}$$

$$y_2 = \beta_1 \sinh(\sqrt{\lambda_2}\, X) + \beta_2 \cosh(\sqrt{\lambda_2}\, X) \tag{105}$$

where coefficients α_1, α_2, β_1, β_2 are to be determined by the corresponding boundary conditions. Afterwards, the two elements of the vector **x** are obtained as,

$$\widetilde{C}_+ = -y_1 + y_2 \tag{106}$$

$$\widetilde{C}_- = y_1 + y_2. \tag{107}$$

The boundary conditions of Eqs. (106) and (107) are as follows. In the bulk solution, $X = X_b$, the electric potential is regarded as the reference, namely, it does not change with the excitation. In addition, all ions have their bulk concentrations which also do not change with the potential perturbation,

$$\widetilde{C}_+ = 0,\ \widetilde{C}_- = 0,\ \widetilde{U} = 0. \tag{108}$$

At the HP, $X = 0$, the boundary conditions are rephrased as,

$$\frac{\partial \widetilde{C}_+}{\partial X} + \frac{\partial \widetilde{U}}{\partial X} = -\frac{\lambda_D \tilde{J}_{de}}{Dc_0} \tag{109}$$

$$\frac{\partial \widetilde{C}_-}{\partial X} - \frac{\partial \widetilde{U}}{\partial X} = 0 \tag{110}$$

$$\widetilde{U}_{HP} = \widetilde{U}_M + \frac{\epsilon_s \delta_{HP}}{\epsilon_{HP} \lambda_D} \frac{\partial \widetilde{U}}{\partial X} \tag{111}$$

where $\tilde{J}_{de}$ is specifically deduced as follows. Firstly, we define,

$$\frac{F\eta}{RT} = \Pi,\ \Pi = \Pi^0 + \widetilde{\Pi} \tag{112}$$

where $\Pi^0 = U_M^0 - U_{HP}^0 - U_{eq}$ is the dimensionless stationary overpotential and $\widetilde{\Pi} = \widetilde{U}_M - \widetilde{U}_{HP}$ the dimensionless perturbation of the potential difference between the electrode surface and the HP.

We consider a reaction of metal ions deposition, $M^+ + e^- \leftrightarrow M$, occurring at the HP. The current density of the reaction, j_{de}, is described by the FBV equation,

$$j_{de} = k_0\left(\exp\left(\frac{\alpha e_0\eta}{k_B T}\right) - \frac{c_{+,HP}}{c_+^0}\exp\left(-\frac{(1-\alpha)e_0\eta}{k_B T}\right)\right) \tag{113}$$

where $c_{+,HP}$ is the concentration of M^+ at the HP, c_+^0 is the concentrations of M^+ in the bulk solution, and k_0 is the reaction rate constant.

Substituting Eqs. (81) and (112) into the FBV theory, Eq. (113), gives,

$$j_{de} = k_0[\exp(\alpha(\Pi^0 + \widetilde{\Pi})) - (C_+^0 + \widetilde{C}_+)\exp(-(1-\alpha)(\Pi^0 + \widetilde{\Pi}))] \tag{114}$$

Expanding Eq. (114) into a first-order Taylor series leads to,

$$j_{de} = k_0[\exp(\alpha\Pi^0)(1 + \alpha\widetilde{\Pi}) - (C_+^0 + \widetilde{C}_+)\exp(-(1-\alpha)\Pi^0)(1-(1-\alpha)\widetilde{\Pi})] \tag{115}$$

Removing the stationary parts and second-order parts, we obtain,

$$\tilde{J}_{de} = k_0[(\alpha\exp(\alpha\Pi^0) + (1-\alpha)C_+^0\exp(-(1-\alpha)\Pi^0))\widetilde{\Pi} - \exp(-(1-\alpha)\Pi^0)\widetilde{C}_+]. \tag{116}$$

Defining two variables related to the reaction rate,

$$\nu_1 = k_0(\alpha\exp(\alpha\Pi^0) + (1-\alpha)C_+^0\exp(-(1-\alpha)\Pi^0)),\ \nu_2 = k_0\exp(-(1-\alpha)\Pi^0) \tag{117}$$

we can reformulate Eq. (116) as,

$$\tilde{J}_{de} = \nu_1(\widetilde{U}_M - \widetilde{U}_{HP}) - \nu_2\widetilde{C}_+ . \tag{118}$$

5.1.4 Impedance Expression

Substituting Eqs. (106)-(107) into the corresponding boundary conditions expressed in Eqs. (108)-(111), we can solve for the four coefficients introduced in Eqs. (104)-(105),

$$\begin{aligned}\alpha_1 = \widetilde{U}_M &\left(-\nu_1 + \frac{2}{r_c + X_b}\frac{Dc_0}{\lambda_D} + \frac{1}{r_c + X_b}\left(\frac{\nu_2\tanh(\sqrt{\lambda_2}X_b)}{\sqrt{\lambda_2}} + \nu_1 X_b\right)\right)/ \\ &\left(-\left(\sqrt{\lambda_1} - \frac{1}{\sqrt{\lambda_1}} + \frac{1}{r_c + X_b}\left(\frac{r_c}{\sqrt{\lambda_1}} + \frac{\tanh(\sqrt{\lambda_1}X_b)}{\lambda_1}\right)\right)\left(2\frac{\lambda_D}{Dc_0} + \frac{1}{\sqrt{\lambda_2}}\nu_2\tanh(\sqrt{\lambda_2}X_b)\right) + \right. \\ &\left.\tanh(\sqrt{\lambda_1}X_b)\left(\frac{\nu_1}{\lambda_1}\frac{r_c}{r_c + X_b} - \nu_2\right) - \frac{r_c X_b}{r_c + X_b}\frac{\nu_1}{\sqrt{\lambda_1}}\right)\end{aligned} \tag{119}$$

$$\alpha_2 = -\alpha_1\tanh(\sqrt{\lambda_1}X_b) \tag{120}$$

$$\beta_1 = -\frac{1}{\sqrt{\lambda_2}}\left(\alpha_1\left(\sqrt{\lambda_1} - \frac{1}{\sqrt{\lambda_1}} + \frac{1}{r_c + X_b}\left(\frac{r_c}{\sqrt{\lambda_1}} + \frac{\tanh(\sqrt{\lambda_1}X_b)}{\lambda_1}\right)\right) + \frac{1}{r_c + X_b}\widetilde{U}_M\right) \tag{121}$$

$$\beta_2 = \frac{1}{\sqrt{\lambda_2}}\left(\alpha_1\left(\sqrt{\lambda_1} - \frac{1}{\sqrt{\lambda_1}} + \frac{1}{r_c + X_b}\left(\frac{r_c}{\sqrt{\lambda_1}} + \frac{\tanh(\sqrt{\lambda_1}X_b)}{\lambda_1}\right)\right) + \frac{1}{r_c + X_b}\widetilde{U}_M\right)\tanh(\sqrt{\lambda_2}X_b) \tag{122}$$

where $r_c = \frac{\epsilon_s\delta_{HP}}{\epsilon_{HP}\lambda_D}$ is the ratio between the Gouy-Chapman capacitance $\left(C_{GC} = \frac{\epsilon_s}{\lambda_D}\right)$ and the Helmholtz capacitance $\left(C_H = \frac{\epsilon_{HP}}{\delta_{HP}}\right)$.

Then we obtain the explicit expression of $\tilde{J}_{de}$ expressed in Eq. (118) by substituting Eqs. (119)-(122) into Eqs. (104) and (107). Besides the reaction current density j_{de}, the EDL current density also needs to be calculated, expressed as,

$$j_{dl} = -\frac{dq_{dl}}{dt} = -\frac{d(F\int_0^{X_b}(c_+ - c_-)dx)}{dt} \tag{123}$$

where q_{dl} is the total charges stored in EDL. The dimensionless form of j_{dl} is,

$$J_{\mathrm{dl}} = -\frac{\mathrm{d}\left(\int_0^{X_\mathrm{b}} (C_+ - C_-)\mathrm{d}X \right)}{\mathrm{d}\tau} \tag{124}$$

Converting Eq. (124) into frequency domain gives,

$$\tilde{J}_{\mathrm{dl}} = -j\omega^{\mathrm{nd}} \int_0^{X_\mathrm{b}} (\tilde{C}_+ - \tilde{C}_-)\mathrm{d}X. \tag{125}$$

The total current density is the sum of the double layer current density and the Faradic reaction current density, namely,

$$\tilde{J} = \tilde{J}_{\mathrm{dl}} + \frac{\lambda_\mathrm{D}}{Dc_0}\tilde{J}_{\mathrm{de}}. \tag{126}$$

So far, we obtain the dimensionless impedance expression,

$$Z^{\mathrm{nd}} = \frac{\tilde{U}_\mathrm{M}}{\tilde{J}} = \frac{r_\mathrm{c}\lambda_1 + X_\mathrm{b}(\lambda_1 - 1) + \dfrac{\tanh(\sqrt{\lambda_1}X_\mathrm{b})}{\sqrt{\lambda_1}} + \sum_{\mathrm{dr}}^{1}}{2j\omega^{\mathrm{nd}}(1 - \mathrm{sech}(\sqrt{\lambda_1}X_\mathrm{b})) + \sum_{\mathrm{dr}}^{2}} \tag{127}$$

where $\sum_{\mathrm{dr}}^{1}$ and $\sum_{\mathrm{dr}}^{2}$ represent the terms related to the coupling of charge transfer reaction and ion transport,

$$\sum_{\mathrm{dr}}^{1} = -\frac{1}{2}\frac{\lambda_\mathrm{D}}{Dc_0} r_\mathrm{c}\nu_1 \left(\frac{\tanh(\sqrt{\lambda_1}X_\mathrm{b})}{\sqrt{\lambda_1}} - X_\mathrm{b} \right) +$$

$$\frac{1}{2}\frac{\lambda_\mathrm{D}}{Dc_0}\nu_2 \left(\left(r_\mathrm{c}\lambda_1 + X_\mathrm{b}(\lambda_1 - 1) + \frac{\tanh(\sqrt{\lambda_1}X_\mathrm{b})}{\sqrt{\lambda_1}} \right) \frac{\tanh(\sqrt{\lambda_2}X_\mathrm{b})}{\sqrt{\lambda_2}} + (r_\mathrm{c} + X_\mathrm{b})\sqrt{\lambda_1}\tanh(\sqrt{\lambda_1}X_\mathrm{b}) \right) \tag{128}$$

$$\sum_{\mathrm{dr}}^{2} = \frac{\lambda_\mathrm{D}}{Dc_0}(\sqrt{\lambda_2}v_2\tanh(\sqrt{\lambda_2}X_\mathrm{b}) - v_1 r_\mathrm{c}\lambda_2)(1 - \mathrm{sech}(\sqrt{\lambda_1}X_\mathrm{b})) + v_1 r_\mathrm{c}\lambda_1\frac{\lambda_\mathrm{D}}{Dc_0} + \frac{\lambda_\mathrm{D}}{Dc_0}v_2\sqrt{\lambda_1}\tanh(\sqrt{\lambda_1}X_\mathrm{b}) \tag{129}$$

Based on previously defined dimensionless variables, we obtain the impedance reference, $Z_{\mathrm{ref}} = \dfrac{2\lambda_\mathrm{D}^2}{DC_{\mathrm{GC}}}$.

Notably, if there is no reaction at the HP, $\nu_1 = \nu_2 = 0$, we obtain $\sum_{\mathrm{dr}}^{1} = \sum_{\mathrm{dr}}^{2} = 0$, and Eq. (127) is reduced to the impedance of an ideal polarizable electrode that has been given in Ref.[58].

5.1.5 Simplifications

Although we have obtained the analytical solution expressed in Eq. (127), it is too complex. Therefore, we need to simplify this expression under some reasonable assumptions. Firstly, in a real system, we have $X_\mathrm{b} \gg 1 \approx r_\mathrm{c}$, then we obtain,

$$\frac{\sum_{\mathrm{dp}}^{1}}{j\omega^{\mathrm{nd}}} \approx \frac{v_1 r_\mathrm{c}}{2}\frac{\lambda_\mathrm{D}}{Dc_0}\left(\frac{X_\mathrm{b}}{j\omega^{\mathrm{nd}}} - \frac{1}{j\omega^{\mathrm{nd}}\sqrt{1 + j\omega^{\mathrm{nd}}}} \right) +$$

$$\frac{v_2}{2}\frac{\lambda_\mathrm{D}}{Dc_0}\left(\frac{1}{j\omega^{\mathrm{nd}}\sqrt{1 + j\omega^{\mathrm{nd}}}}\frac{\tanh(\sqrt{j\omega^{\mathrm{nd}}}X_\mathrm{b})}{\sqrt{j\omega^{\mathrm{nd}}}} + X_\mathrm{b}\left(\frac{\sqrt{1 + j\omega^{\mathrm{nd}}}}{j\omega^{\mathrm{nd}}} + \frac{\tanh(\sqrt{j\omega^{\mathrm{nd}}}X_\mathrm{b})}{\sqrt{j\omega^{\mathrm{nd}}}} \right) \right) \tag{130}$$

$$\frac{\sum_{\mathrm{dp}}^{2}}{j\omega^{\mathrm{nd}}} \approx \frac{\lambda_\mathrm{D}}{Dc_0}\left(\frac{v_2\tanh(\sqrt{j\omega^{\mathrm{nd}}}X_\mathrm{b})}{\sqrt{j\omega^{\mathrm{nd}}}} - v_1 r_\mathrm{c} \right) + v_1 r_\mathrm{c}\frac{\lambda_\mathrm{D}}{Dc_0} + \frac{v_1 r_\mathrm{c}}{j\omega^{\mathrm{nd}}}\frac{\lambda_\mathrm{D}}{Dc_0} + \frac{\lambda_\mathrm{D}}{Dc_0}v_2\frac{\sqrt{1 + j\omega^{\mathrm{nd}}}}{j\omega^{\mathrm{nd}}} \tag{131}$$

Substituting Eqs. (130) and (131) into Eq. (127) leads,

$$Z^{\mathrm{nd}} = \frac{X_\mathrm{b}}{2} + \frac{\left(\dfrac{r_\mathrm{c}}{j\omega^{\mathrm{nd}}} + \dfrac{1}{j\omega^{\mathrm{nd}}\sqrt{j\omega^{\mathrm{nd}} + 1}} \right) + \dfrac{\lambda_\mathrm{D}}{Dc_0}\dfrac{1}{j\omega^{\mathrm{nd}}\sqrt{1 + j\omega^{\mathrm{nd}}}}\left(\dfrac{v_2}{2}\dfrac{\tanh(\sqrt{j\omega^{\mathrm{nd}}}X_\mathrm{b})}{\sqrt{j\omega^{\mathrm{nd}}}} - \dfrac{v_1 r_\mathrm{c}}{2} \right)}{2 + v_2\dfrac{\lambda_\mathrm{D}}{Dc_0}\left(\dfrac{\tanh(\sqrt{j\omega^{\mathrm{nd}}}X_\mathrm{b})}{\sqrt{j\omega^{\mathrm{nd}}}} + \dfrac{\sqrt{1 + j\omega^{\mathrm{nd}}}}{j\omega^{\mathrm{nd}}} \right) + v_1 r_\mathrm{c}\dfrac{\lambda_\mathrm{D}}{Dc_0}\dfrac{1}{j\omega^{\mathrm{nd}}}}. \tag{132}$$

Usually, $\omega^{\mathrm{nd}} = \omega\dfrac{\lambda_\mathrm{D}^2}{D} \approx \omega \times 10^{-9} \ll 1$, then we obtain,

$$Z^{nd}=\frac{X_b}{2}+\frac{\left(\frac{r_c}{j\omega^{nd}}+\frac{1}{j\omega^{nd}\sqrt{j\omega^{nd}+1}}\right)+\frac{\lambda_D}{Dc_0}\frac{1}{j\omega^{nd}\sqrt{1+j\omega^{nd}}}\left(\frac{v_2}{2}\frac{\tanh(\sqrt{j\omega^{nd}}X_b)}{\sqrt{j\omega^{nd}}}-\frac{v_1r_c}{2}\right)}{2+v_2\frac{\lambda_D}{Dc_0}\left(\frac{\tanh(\sqrt{j\omega^{nd}}X_b)}{\sqrt{j\omega^{nd}}}+\frac{\sqrt{1+j\omega^{nd}}}{j\omega^{nd}}\right)+v_1r_c\frac{\lambda_D}{Dc_0}\frac{1}{j\omega^{nd}}}$$

$$\approx\frac{X_b}{2}+\frac{\frac{1+r_c}{j\omega^{nd}}+\frac{\lambda_D}{Dc_0}\frac{1}{j\omega^{nd}}\left(\frac{v_2}{2}\frac{\tanh(\sqrt{j\omega^{nd}}X_b)}{\sqrt{j\omega^{nd}}}-\frac{v_1r_c}{2}\right)}{2+v_2\frac{\lambda_D}{Dc_0}\frac{\tanh(\sqrt{j\omega^{nd}}X_b)}{\sqrt{j\omega^{nd}}}+\frac{\lambda_D}{Dc_0}\frac{1}{j\omega^{nd}}(v_1r_c+v_2)}$$

$$=\frac{X_b}{2}+\frac{1}{2}\frac{1}{\frac{j\omega^{nd}}{1+r_c}+\frac{j\omega^{nd}\left(\frac{r_c}{1+r_c}\frac{\lambda_D}{Dc_0}\frac{v_2}{2}\frac{\tanh(\sqrt{j\omega^{nd}}X_b)}{\sqrt{j\omega^{nd}}}+\frac{v_2}{2}\frac{\lambda_D}{Dc_0}\frac{1}{j\omega^{nd}}+\frac{1}{1+r_c}\frac{\lambda_D}{Dc_0}\frac{v_1r_c}{2}+\frac{1}{j\omega^{nd}}\frac{\lambda_D}{Dc_0}\frac{v_1r_c}{2}\right)}{1+r_c+\frac{\lambda_D}{Dc_0}\left(\frac{v_2}{2}\frac{\tanh(\sqrt{j\omega^{nd}}X_b)}{\sqrt{j\omega^{nd}}}-\frac{v_1r_c}{2}\right)}}$$

$$=\frac{X_b}{2}+\frac{1}{2}\frac{1}{\frac{j\omega^{nd}}{1+r_c}+\frac{1}{\frac{2}{v_2}\frac{Dc_0}{\lambda_D}(1+r_c)-\frac{v_1r_c}{v_2}+\frac{\tanh(\sqrt{j\omega^{nd}}X_b)}{\sqrt{j\omega^{nd}}}}} \tag{133}$$

We notice that the final expression of Eq. (133) has a coefficient of $\frac{1}{2}$, which may look a little weird to readers. Therefore, we redefine the impedance reference as $\frac{\lambda_D{}^2}{DC_{GC}}$, then Eq. (133) is reformulated as,

$$Z^{nd}=X_b+\frac{1}{\frac{j\omega^{nd}}{1+r_c}+\frac{1}{\frac{2}{v_2}\frac{Dc_0}{\lambda_D}(1+r_c)-\frac{v_1r_c}{v_2}+\frac{\tanh(\sqrt{j\omega^{nd}}X_b)}{\sqrt{j\omega^{nd}}}}} \tag{134}$$

We define, $R_s^{nd}=X_b$ the dimensionless solution resistance, $R_{ct}^{nd}=\frac{2}{v_2}\frac{Dc_0}{\lambda_D}(1+r_c)-\frac{v_1r_c}{v_2}$ the dimensionless charge transfer resistance and $W^{nd}=\frac{\tanh(\sqrt{j\omega^{nd}}X_b)}{\sqrt{j\omega^{nd}}}$ the dimensionless Warburg impedance. Eq.(134) embodies the coupling relationships between charge transfer reaction and EDL charging. Specifically, both R_{ct}^{nd} and C_{dl}^{nd} have the capacitance ratio term, r_c.

Then Eq. (133) is reformulated as,

$$Z^{nd}=R_s^{nd}+\frac{1}{j\omega^{nd}C_{dl}^{nd}+\frac{1}{R_{ct}^{nd}+W^{nd}}} \tag{135}$$

From this simplified condition, we define the characteristic frequency of charge transfer reaction as, $\omega_{ct}^{nd}=\frac{1}{R_{ct}^{nd}C_{dl}^{nd}}$, and the characteristic frequency of diffusion as, $\omega_d=\frac{D}{x_b^2}$, whose dimensionless form is $\omega_d^{nd}=\frac{1}{X_b^2}$.

When $\omega^{nd}<\omega_d^{nd}$, Eq. (135) is simplified to,

$$Z^{nd}=R_s^{nd}+\frac{\tanh(\sqrt{j\omega^{nd}}X_b)}{\sqrt{j\omega^{nd}}} \tag{136}$$

whose Nyquist plot is a 45°-line followed by a semi-circle, as shown in Figure 11(D), representing ion diffusion in bulk solution.

When $\omega_d^{nd} < \omega^{nd} < \omega_{ct}^{nd}$, Eq. (136) is reduced to,

$$Z^{nd} = R_s^{nd} + \frac{1}{j\omega^{nd}C_{dl}^{nd} + \frac{1}{R_{ct}^{nd}}} \tag{137}$$

whose Nyquist plot is an ideal semi-circle, as shown in Figure 11(C), representing the charge transfer reaction.

Finally, when $\omega^{nd} > \omega_{ct}^{nd}$, Eq. (137) is reduced to,

$$Z^{nd} = R_s^{nd} + \frac{1}{j\omega^{nd}C_{dl}^{nd}} \tag{138}$$

whose Nyquist plot is a straight line representing the EDL charging process, as shown in Figure 11(B).

5.2 Numerical Methods of Impedance Calculation

In this section, we introduce the methods of calculating the impedance from time-domain data, which can be obtained from models and experiments. Firstly, the method of an analytical Fourier transform (AFT) is introduced[59]. Then it is used to calculate the impedance of the deposition reaction of metal ions. Lastly, the fast Fourier transform (FFT), another often used numerical method, is introduced briefly.

5.2.1 Analytical Fourier transform

Applying linear interpolation to time-domain signal, we obtain

$$\hat{h}(t) = \left(\sigma(t) - \sigma\left(t - \sum_{i=1}^{1}\Delta t_i\right)\right)\cdot\left(h_1 + \frac{h_2 - h_1}{\Delta t_1}t\right) + \ldots + \left(\sigma\left(t - \sum_{i=1}^{n-2}\Delta t_i\right) - \sigma\left(t - \sum_{i=1}^{n-1}\Delta t_i\right)\right)\cdot\left(h_{n-1} + \frac{h_n - h_{n-1}}{\Delta t_{n-1}}\left(t - \sum_{i=1}^{n-2}\Delta t_i\right)\right) \tag{139}$$

where $h(t)$ is the recorded time-domain signal, $\sigma(t)$ the normalized step function. Then applying Fourier transform to Eq. (139) gives,

$$\begin{aligned}
\hat{H}(\omega) &= \int_0^{\infty}\hat{h}(t)\exp(-j\omega t)\mathrm{d}t \\
&= \frac{1}{j\omega}\left(h_1 - h_n\exp\left(-j\omega\sum_{i=1}^{n-1}\Delta t_i\right)\right) - \frac{1}{\omega^2}\left(\frac{h_2 - h_1}{\Delta t_1} - \frac{h_n - h_{n-1}}{\Delta t_{n-1}}\exp\left(-j\omega\sum_{i=1}^{n-1}\Delta t_i\right)\right) \\
&\quad - \frac{1}{\omega^2}\sum_{k=1}^{n-2}\left(\frac{h_{k+2} - h_{k+1}}{\Delta t_{k+1}} - \frac{h_{k+1} - h_k}{\Delta t_k}\right)\exp\left(-j\omega\sum_{i=1}^{k}\Delta t_i\right)
\end{aligned} \tag{140}$$

where the specific derivations are detailed below. Integrating the last term of $\hat{h}(t)$ gives,

$$\begin{aligned}
\hat{H}_{n-1}(\omega) &= \int_0^{\infty}\hat{h}(t)\exp(-j\omega t)\mathrm{d}t \\
&= \int_0^{\infty}\left(\sigma\left(t - \sum_{i=1}^{n-2}\Delta t_i\right) - \sigma\left(t - \sum_{i=1}^{n-1}\Delta t_i\right)\right)\cdot\left(h_{n-1} + \frac{h_n - h_{n-1}}{\Delta t_{n-1}}\left(t - \sum_{i=1}^{n-2}\Delta t_i\right)\right)\exp(-j\omega t)\mathrm{d}t \\
&= \int_{\sum_{i=1}^{n-2}\Delta t_i}^{\sum_{i=1}^{n-1}\Delta t_i}\left(h_{n-1} + \frac{h_n - h_{n-1}}{\Delta t_{n-1}}\left(t - \sum_{i=1}^{n-2}\Delta t_i\right)\right)\exp(-j\omega t)\mathrm{d}t \\
&= h_{n-1}\int_{\sum_{i=1}^{n-2}\Delta t_i}^{\sum_{i=1}^{n-1}\Delta t_i}\exp(-j\omega t)\mathrm{d}t + \frac{h_n - h_{n-1}}{\Delta t_{n-1}}\int_{\sum_{i=1}^{n-2}\Delta t_i}^{\sum_{i=1}^{n-1}\Delta t_i}t\exp(-j\omega t)\mathrm{d}t - \frac{h_n - h_{n-1}}{\Delta t_{n-1}}\sum_{i=1}^{n-2}\Delta t_i\int_{\sum_{i=1}^{n-2}\Delta t_i}^{\sum_{i=1}^{n-1}\Delta t_i}\exp(-j\omega t)\mathrm{d}t \\
&= -\frac{1}{j\omega}h_{n-1}\left(\exp\left(-j\omega\sum_{i=1}^{n-1}\Delta t_i\right) - \exp\left(-j\omega\sum_{i=1}^{n-2}\Delta t_i\right)\right) \\
&\quad + \frac{h_n - h_{n-1}}{\Delta t_{n-1}}\left(\frac{1}{\omega^2}\left(\exp\left(-j\omega\sum_{i=1}^{n-1}\Delta t_i\right) - \exp\left(-j\omega\sum_{i=1}^{n-2}\Delta t_i\right)\right) - \frac{1}{j\omega}\left(\sum_{i=1}^{n-1}\Delta t_i\exp\left(-j\omega\sum_{i=1}^{n-1}\Delta t_i\right) - \sum_{i=1}^{n-2}\Delta t_i\exp\left(-j\omega\sum_{i=1}^{n-2}\Delta t_i\right)\right)\right)
\end{aligned}$$

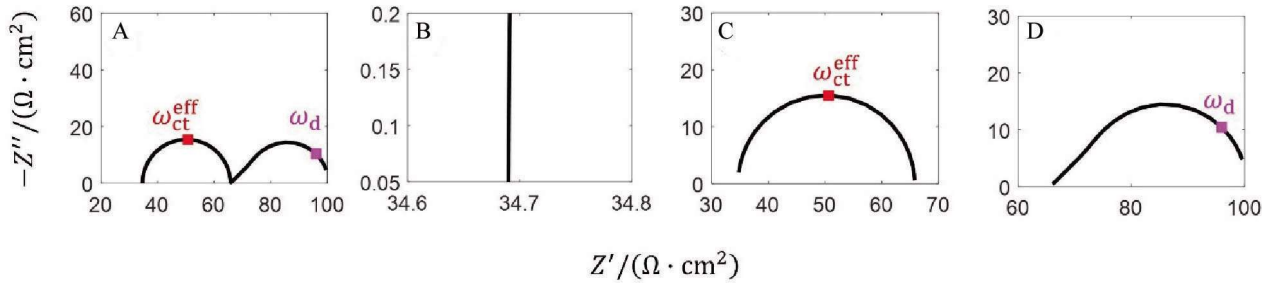

Figure 11 Nyquist plots of simplified impedance in different frequency ranges. (A) Full frequency range, 1×10^{6} Hz ~ 1×10^{-4} Hz; (B) $\omega^{nd} > \omega_{ct}^{nd}$, 1×10^{6} Hz ~ 1×10^{5} Hz; (C) $\omega_d^{nd} < \omega^{nd} < \omega_{ct}^{nd}$, 1×10^{4} Hz ~ 10 Hz; (D) $\omega^{nd} < \omega_d^{nd}$, 1 Hz ~ 1×10^{-4} Hz. Parameters are c_0 = 100 mol·m^{-3}, $k_0 = 3\times10^{-4}$ mol·m^{-2}·s^{-1}, $D = 1\times10^{-10}$ m^2·s^{-1}. Matlab script of this model is provided in the supporting information. (color on line)

$$+\frac{1}{j\omega}\frac{h_n-h_{n-1}}{\Delta t_{n-1}}\sum_{i=1}^{n-2}\Delta t_i\left(\exp\left(-j\omega\sum_{i=1}^{n-1}\Delta t_i\right)-\exp\left(-j\omega\sum_{i=1}^{n-2}\Delta t_i\right)\right)$$
$$=-\frac{1}{j\omega}h_{n-1}\left(\exp\left(-j\omega\sum_{i=1}^{n-1}\Delta t_i\right)-\exp\left(-j\omega\sum_{i=1}^{n-2}\Delta t_i\right)\right)+\frac{1}{\omega^2}\frac{h_n-h_{n-1}}{\Delta t_{n-1}}\left(\left(\exp\left(-j\omega\sum_{i=1}^{n-1}\Delta t_i\right)-\exp\left(-j\omega\sum_{i=1}^{n-2}\Delta t_i\right)\right)\right)$$
$$+\frac{1}{j\omega}\frac{h_n-h_{n-1}}{\Delta t_{n-1}}\exp\left(-j\omega\sum_{i=1}^{n-1}\Delta t_i\right)\left(\sum_{i=1}^{n-2}\Delta t_i-\sum_{i=1}^{n-1}\Delta t_i\right) \tag{141}$$

Similarly, we obtain the frequency-domain expression for each term of Eq. (139),

$$\hat{H}_{n-2}(\omega)=\frac{1}{j\omega}h_{n-2}\exp\left(-j\omega\sum_{i=1}^{n-3}\Delta t_i\right)+\frac{1}{\omega^2}\frac{h_{n-1}-h_{n-2}}{\Delta t_{n-2}}\left(\left(\exp\left(-j\omega\sum_{i=1}^{n-2}\Delta t_i\right)-\exp\left(-j\omega\sum_{i=1}^{n-3}\Delta t_i\right)\right)\right)-\frac{1}{j\omega}h_{n-1}\exp\left(-j\omega\sum_{i=1}^{n-2}\Delta t_i\right)$$

……

$$\hat{H}_2(\omega)=\frac{1}{j\omega}h_2\exp\left(-j\omega\sum_{i=1}^{1}\Delta t_i\right)+\frac{1}{\omega^2}\frac{h_3-h_2}{\Delta t_{n-2}}\left(\left(\exp\left(-j\omega\sum_{i=1}^{2}\Delta t_i\right)-\exp\left(-j\omega\sum_{i=1}^{1}\Delta t_i\right)\right)\right)-\frac{1}{j\omega}h_3\exp\left(-j\omega\sum_{i=1}^{2}\Delta t_i\right)$$

$$\hat{H}_1(\omega)=\frac{1}{j\omega}h_1+\frac{1}{\omega^2}\frac{h_2-h_1}{\Delta t_1}\left(\left(\exp\left(-j\omega\sum_{i=1}^{1}\Delta t_i\right)-1\right)\right)-\frac{1}{j\omega}h_2\exp\left(-j\omega\sum_{i=1}^{1}\Delta t_i\right) \tag{142}$$

Adding up all terms from $\hat{H}_1(\omega)$ to $\hat{H}_{n-1}(\omega)$, we obtain Eq. (140).

5.2.2 Application of AFT

Figure 12 compares the AFT-calculated and the analytical impedance expressed in Eq. (127). Notice that the results of AFT have some deviation in the entire frequency range. Especially, the deviation in the limiting high-frequency region is more obvious. The main reason is that the AFT method accumulates error in the numerical calculations. Due to the fact that the AFT calculation is a quite time-consuming task in a low frequency range, current results only show a 45°-line without a semi-circle that should occur in the low-frequency region.

Except for the AFT method, another often-used Fourier transform method is the FFT, which is widely used in signal processing[60]. However, FFT is a completely pure numerical method. Compared with AFT, it lacks stability and has higher requirements for the signal-noise ratio of the time-domain signal.

6 Conclusions

This paper is designed as a tutorial tool on EDL modelling, including equilibrium models (the GCS model and the BPB model), nonequilibrium models (PNP-like models), and models under AC conditions (the EIS

models). Exposition of these models begins with physical insights, followed by detailed mathematical derivation, formal analysis, and then practical numerical implementation with the Matlab scripts provided in the supporting information. A viable attempt to craft a physical model for the specific system under one's own investigation could start with following the model development procedure presented here with pencil and paper.

Acknowledgements:

This work is financially supported by National Natural Science Foundation of China (21802170) and the Alexander von Humboldt Foundation.

Notes:

The authors declare no competing financial interests.

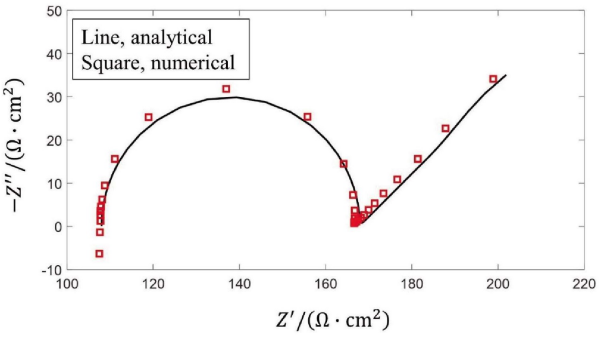

Figure 12 Comparison between the AFT-calculated and the analytical impedance expressed in Eq. (127). Parameters used in calculation are as follows, c_0 = 100 mol·m^{-3}, k_0 = 4.45× 10^{-5} mol·m^{-2}·s^{-1}, D = 3.2×10^{-11} m^2·s^{-1}, frequency range: 4.22×10^{-4} ~ 5×10^5 Hz, sampling frequency: 100*(excitation frequency), sampling duration: the reciprocal of sampling frequency. Matlab script of this model is provided in the supporting information.

References:

[1] Huang J, Chen S L, Eikerling M. Grand-canonical model of electrochemical double layers from a hybrid density-potential functional[J]. J. Chem. Theory Comput., 2021, 17(4): 2417-2430.

[2] Trasatti S, Lust E. The potential of zero charge, in Modern aspects of electrochemistry[M]. White R E, Bockris J O' M, Conway B E, Editors, 1999, Springer US: Boston, MA. 1-215.

[3] Schmickler W, Guidelli R. The partial charge transfer[J]. Electrochim. Acta, 2014, 127: 489-505.

[4] Huang J, Malek A, Zhang J B, Eikerling M. Non-monotonic surface charging behavior of platinum: A paradigm change[J]. J. Phys. Chem. C, 2016, 120(25): 13587-13595.

[5] Huang J, Zhou T, Zhang J B, Eikerling M. Double layer of platinum electrodes: Non-monotonic surface charging phenomena and negative double layer capacitance[J]. J. Chem. Phys., 2018, 148(4): 044704.

[6] Helmholtz H V. Studien über electrische grenzschichten[J]. Ann. Phys., 1879, 243(7): 337-382.

[7] Chapman D L, Li. A contribution to the theory of electrocapillarity[J]. Philos. Mag., 1913, 25(148): 475-481.

[8] Gouy G. Sur la constitution de la charge electrique a la surface d'un electrolyte.[J]. J. Phys. Theor. Appl., 1910, 9(1): 457-468.

[9] Stern O. Zur theorie der elektrolytischen doppelschicht[J]. Ber. Bunsenges. Phys. Chem., 1924, 30(21-22): 508-516.

[10] Bikerman J J. Xxxix. Structure and capacity of electrical double layer[J]. Lond. Edinb. Dubl. Phil. Mag., 1942, 33(220): 384-397.

[11] Grahame D C. The electrical double layer and the theory of electrocapillarity[J]. Chem. Rev., 1947, 41(3): 441-501.

[12] Lobenz W, Salie G. Potentialabhängigkeit und ladungsübergangskoeffizienten der tl/tl+-reaktion[J]. Z. Phys. Chem., 1961, 29(5): 408-412.

[13] Grahame D C. Components of charge and potential in the non-diffuse region of the electrical double layer: Potassium iodide solutions in contact with mercury at 25°[1][J]. J. Am. Chem. Soc., 1958, 80(16): 4201-4210.

[14] Mott N F, Watts-Tobin R J. The interface between a metal and an electrolyte[J]. Electrochim. Acta, 1961, 4(2): 79-107.

[15] Mott N F, Parsons R, Watts-Tobin R J. The capacity of a mercury electrode in electrolytic solution[J]. Philos. Mag., 1962, 7 (75): 483-493.

[16] Watts-tobin R J. The interface between a metal and an electrolytic solution[J]. Philos. Mag., 1961, 6(61): 133-153.

[17] Schmickler W. Electronic effects in the electric double layer[J]. Chem. Rev., 1996, 96(8): 3177-3200.

[18] Guidelli R, Schmickler W. Recent developments in models for the interface between a metal and an aqueous solution [J]. Electrochim. Acta, 2000. 45(15): 2317-2338.

[19] Trasatti S. Effect of the nature of the metal on the dielectric properties of polar liquids at the interface with electrodes. A

phenomenological approach[J]. J. Electroanal. Chem. Interfacial Electrochem., 1981, 123(1): 121-139.

[20] Badiali J P, Rosinberg M L, Vericat F, Blum L. A microscopic model for the liquid metal-ionic solution interface[J]. J. Electro-Anal. Chem., 1983, 158(2): 253-267.

[21] Kornyshev A A. Metal electrons in the double layer theory[J]. Electrochim. Acta, 1989, 34(12): 1829-1847.

[22] Schmickler W. A jellium-dipole model for the double layer[J]. J. Electroanal. Chem., 1983, 150(1): 19-24.

[23] Lundqvist S, March N H. Theory of the inhomogeneous electron gas[M]//Physics of solids and liquids, Springer Science & Business Media. XIV, Plenum Press, New York, 1983: 396.

[24] Price D L, Halley J W. Molecular dynamics, density functional theory of the metal-electrolyte interface[J]. J. Chem. Phys., 1995, 102(16): 6603-6612.

[25] Otani M, ugino O. First-principles calculations of charged surfaces and interfaces: A plane-wave nonrepeated slab approach[J]. Phys. Rev. B, 2006, 73(11): 115407.

[26] Petrosyan S A, Briere J F, Roundy D, Arias T A. Joint density-functional theory for electronic structure of solvated systems[J]. Phys. Rev. B, 2007, 75(20): 205105.

[27] Letchworth-Weaver K, Arias T A. Joint density functional theory of the electrode-electrolyte interface: Application to fixed electrode potentials, interfacial capacitances, and potentials of zero charge[J]. Phys. Rev. B, 2012, 86(7): 075140.

[28] Sundararaman R, Goddard W A, Arias T A. Grand canonical electronic density-functional theory: Algorithms and applications to electrochemistry[J]. J. Chem. Phys., 2017, 146(11): 114104.

[29] Jinnouchi R, Anderson A B. Electronic structure calculations of liquid-solid interfaces: Combination of density functional theory and modified Poisson-Boltzmann theory[J]. Phys. Rev. B, 2008, 77(24): 245417.

[30] Mathew K, Sundararaman R, Letchworth-Weaver K, Arias T A, Hennig R G. Implicit solvation model for density functional study of nanocrystal surfaces and reaction pathways[J]. J. Chem. Phys., 2014, 140(8): 084106.

[31] Mathew K, Kolluru V S C, Mula S, Steinmann S N, Hennig R G. Implicit self-consistent electrolyte model in plane-wave density-functional theory[J]. J. Chem. Phys., 2019, 151(23): 234101.

[32] Nishihara S, Otani M. Hybrid solvation models for bulk, interface, and membrane: Reference interaction site methods coupled with density functional theory[J]. Phys. Rev. B, 2017, 96(11): 115429.

[33] Nattino F, Truscott M, Marzari N, Andreussi O. Continuum models of the electrochemical diffuse layer in electronic structure calculations[J]. J. Chem. Phys., 2018, 150(4): 041722.

[34] Hörmann N G, Andreussi O, Marzari N. Grand canonical simulations of electrochemical interfaces in implicit solvation models[J]. J. Chem. Phys., 2019, 150(4): 041730.

[35] Melander M M, Kuisma M J, Christensen T E K, Honkala K. Grand-canonical approach to density functional theory of electrocatalytic systems: Thermodynamics of solid-liquid interfaces at constant ion and electrode potentials[J]. J. Chem. Phys., 2018, 150(4): 041706.

[36] Le J B, Iannuzzi M, Cuesta A, Cheng J. Determining potentials of zero charge of metal electrodes versus the standard hydrogen electrode from density-functional-theory-based molecular dynamics[J]. Phys. Rev. Lett., 2017, 119(1): 016801.

[37] Sakong S, Groβ A, The electric double layer at metal water interfaces revisited based on a charge polarization scheme[J]. J. Chem. Phys., 2018, 149(8): 084705.

[38] Sakong S, Groβ A. Water structures on a Pt(111) electrode from ab initio molecular dynamic simulations for a variety of electrochemical conditions[J]. Phys. Chem. Chem. Phys., 2020, 22(19): 10431-10437.

[39] Le J B, Chen A, Li L, Xiong J F, Lan J G, Liu Y P, Iannuzzi M, Cheng J. Modeling electrified Pt(111)-Had/water interfaces from *ab initio* molecular dynamics[J]. JACS Au, 2021, 1(5): 569-577.

[40] Huang J, Li P, Chen S L.Potential of zero charge and surface charging relation of metal-solution interphases from a constant-potential Jellium-Poisson-Boltzmann model[J]. Phys. Rev. B, 2020, 101(12): 125422.

[41] Huang J. Hybrid density-potential functional theory of electric double layers[J]. Electrochim. Acta, 2021, 389: 138720.

[42] Karasiev V V, Trickey S B. Chapter nine-frank discussion of the status of ground-state orbital-free DFT[M]//Advances in quantum chemistry. Sabin J R, Cabrera-Trujillo R, Editors, Academic Press, 2015: 221-245.

[43] Wang Y A, Carter E A. Orbital-free kinetic-energy density functional theory, in Theoretical methods in condensed phase chemistry[M]. Schwartz S D, Editor, Springer Netherlands: Dordrecht, 2002: 117-184.

[44] Gavini V, Bhattacharya K, Ortiz M. Quasi-continuum orbital-free density-functional theory: A route to multi-million atom

non-periodic DFT calculation[J]. J. Mech. Phys. Solids, 2007, 55(4): 697-718.

[45] Nightingale E R. Phenomenological theory of ion solvation. Effective radii of hydrated ions[J]. J. Phys. Chem., 1959, 63(9): 1381-1387.

[46] Bazant M Z, Kilic M S, Storey B D, Ajdari A. Towards an understanding of induced-charge electrokinetics at large applied voltages in concentrated solutions[J]. Adv. Colloid Interface, 2009, 152(1-2): 48-88.

[47] Kornyshev A A. Double-layer in ionic liquids: Paradigm change?[J]. J. Phys. Chem. B, 2007, 111(20): 5545-5557.

[48] Zhang Y F, Huang J. Treatment of ion-size asymmetry in lattice-gas models for electrical double layer[J]. J. Phys. Chem. C, 2018, 122(50): 28652-28664.

[49] Zhang L L, Cai J, Chen Y X, Huang J. Modelling electrocatalytic reactions with a concerted treatment of multistep electron transfer kinetics and local reaction conditions[J]. J. Phys. Condens. Mat., 2021, 33(50): 504002.

[50] Zhang Z M, Gao Y, Chen S L, Huang J. Understanding dynamics of electrochemical double layers via a modified concentrated solution theory[J]. J. Electrochem. Soc., 2019. 167(1): 013519.

[51] Budkov Y A. Nonlocal statistical field theory of dipolar particles in electrolyte solutions[J]. J. Phys. Condens. Mat., 2018, 30(34): 344001.

[52] Budkov Y A. Statistical field theory of ion-molecular solutions[J]. Phys. Chem. Chem. Phys., 2020, 22(26): 14756-14772.

[53] Huang J. Confinement induced dilution: Electrostatic screening length anomaly in concentrated electrolytes in confined space [J]. J. Phys. Chem. C, 2018, 122(6): 3428-3433.

[54] Gao Y, Huang J, Liu Y W, Yan J W, Mao B W, Chen S L. Ion-vacancy coupled charge transfer model for ion transport in concentrated solutions[J]. Sci. China. Chem., 2019, 62(4): 515-520.

[55] Bard A J, Faulkner L R. Electrochemical methods: Fundamentals and applications[M]. 2nd ed. Russ. J. Electrochem., New York: Wiley, 2002, 38: 1364-1365.

[56] Bockris J O'm, Devanathan M A V, Müller K. On the structure of charged interfaces[J]. Roy. Soc. A, 1963, 274(541): 55-79.

[57] Huang J, Li Z, Liaw B Y, Zhang J B. Graphical analysis of electrochemical impedance spectroscopy data in bode and Nyquist representations[J]. J. Power Sources, 2016, 309: 82-98.

[58] Li C K, Huang J. Impedance response of electrochemical interfaces: Part i. Exact analytical expressions for ideally polarizable electrodes[J]. J. Electrochem. Soc., 2021, 167(16): 166517.

[59] Klotz D, Schönleber M, Schmidt J, Ivers-Tiffée E. New approach for the calculation of impedance spectra out of time domain data[J]. Electrochim. Acta, 2011, 56(24): 8763-8769.

[60] Nussbaumer H J. The fast fourier transform, in fast fourier transform and convolution algorithms[M]. Nussbaumer H J, Editor, Springer Berlin Heidelberg: Berlin, Heidelberg, 1981: 80-111.

平衡、非平衡、交流状态下电化学双电层建模的初学者指南

张露露[1#],李琛坤[2#],黄 俊[3*]

(1. 中国科学技术大学化学与材料科学学院,安徽 合肥 230026,中华人民共和国;
2. 中南大学化学化工学院,湖南 长沙 410083,中华人民共和国; 3.乌尔姆大学理论化学研究所,乌尔姆 89069,德国)

摘要: 本文定位在一篇电化学双电层(EDL)理论建模方面入门级文章。我们首先简要介绍了 EDL 的基本特征,简述了 EDL 理论建模的发展历史,特别是 D.C. Grahame 之后近几十年的发展历史。然后,我们依次介绍了平衡状态和动态下不同复杂度的 EDL 模型。作为一篇入门级文章,我们尽可能详细地阐释理论模型的物理图像、假设、数学推导、形式分析、数值分析,并附上 Matlab 仿真代码。平衡状态下的模型包括 Gouy-Chapman-Stern(GCS)模型,Bikerman-Poisson-Boltzmann(BPB)模型,和非对称离子尺寸模型。我们强调 GCS 模型和 BPB 模型在处理离子有限尺寸上存在一个微妙的不同。GCS 模型通过人为引入 Helmholtz 平面来考虑离子有限尺寸,但在 Helmholtz 平面内及弥散层内却依然采用没有考虑离子尺寸效应的 Poisson-Boltzmann 理论,因而此处的离子浓度可以无限大。与之不同,BPB 模型通过格子气体方法,能够自洽描述离子有限尺寸效应。不同以往直接采用 Poisson-Nernst-Planck 方程描述 EDL 动态行为,我们从 EDL 的巨势出发,运用基本的泛函分析方法,推导了一个考虑离子有限尺寸的 EDL 动态模型。这一理论方法拓展性好。读者可以根据研究对象的需要,建立不同复杂度的 EDL 动态模型。最后,我们基于 EDL 动态模型,推导了 EDL 的电化学阻抗谱理论模型,以试图向读者展示如何从一个时域物理模型出发,推导相应的阻抗谱物理模型。读者若想要踏进理论电化学这个美丽的花园,根据我们自己学习和研究的经验,一个可行的方式是拿起纸和笔来开始推导本文所介绍的这些模型。

关键词: 双电层;平衡;非平衡;电化学阻抗谱;物理建模